The Role of Organic Matter Diversity on the Re-Os Systematics of Organic-rich Sedimentary Units: Insights into the Controls of Isochron Age Determinations from the Lacustrine Green River Formation

Jeffrey T. Pietras[1], *Abby Dennett*[1], *David Selby*[2], *Justin E. Birdwell*[3]

[1]*Department of Geological Sciences and Environmental Studies, Binghamton University, 4400 Vestal Pkwy E, Binghamton, NY 13902, USA*

[2]*Department of Earth Sciences, Durham University, Stockton Road, Durham DH1 3LE, UK*

[3]*U.S. Geological Survey, Central Energy Resources Science Center, Denver Federal Center, MS 939, Denver, CO 80225*

corresponding author: Jeffrey T. Pietras jpietras@binghamton.edu

Abstract

The range of $^{187}Re/^{188}Os$ values measured from samples of five organic-rich lacustrine mudstones units in the Eocene Green River Formation in the easternmost Uinta Basin covaries with organic matter diversity driven by changing water column conditions. A set of samples from the Douglas Creek Member has the highest pristane/phytane ratio and lowest β-carotane/*n*-C_{30} ratio compared to overlying units indicating deposition in an oxic-anoxic environment with low salinity that would have allowed for the accumulation of a diverse assemblage of aquatic organisms. These samples define the broadest $^{187}Re/^{188}Os$ range of 1504. In contrast, samples from the R6 and Mahogany zones possess lower pristane/phytane ratios and higher β-carotane/*n*-C_{30} ratios indicating deposition in a more restricted lacustrine environment with elevated salinities and alkalinities that would have limited aquatic organic matter diversity. The R6 and

Mahogany zones have the narrowest range of $^{187}Re/^{188}Os$ values measured in this study of 254.9 and 154.6, respectively. As noted by previous workers, these results suggest that organic matter diversity plays a primary role in determining the range of $^{187}Re/^{188}Os$ ratios in a sample set, and in turn the uncertainty of Re-Os age determinations from organic-rich sedimentary rocks.

The Re-Os data from the R3 zone and R6 zone yield ages of 49.7 ±3.4 Ma and 42.0 ±18 Ma, respectively, which are statistically indistinguishable based on 2σ uncertainty from three previously reported Re-Os age determinations and those provided by $^{40}Ar/^{39}Ar$ geochronology of interbedded volcanic ash beds. Although the age uncertainty is high, these findings further highlight the importance of Re-Os geochronology in lacustrine basins, particularly those with thick mudstone successions that lack volcanic ash layers, reliable biostratigraphy, or magnetostratigraphic control. In these cases, even ages with large uncertainties can be useful to constrain burial history and thermal history models.

Together, the initial $^{187}Os/^{188}Os$ ratios of five sets of samples analyzed from the Uinta Basin define the largest Os isotope stratigraphic record from any lacustrine basin compiled to date and record a shift from a value of 1.40 to 1.48 between the R3 and R4 zones in the lower part of the Parachute Creek Member. This small shift may signify a change in the chemical weathering products that entered the lake preserved 20 to 50 meters above the contact between the Douglas Creek and the lower Parachute Creek members during a period when the basin transitioned from a shallow lake with mostly open hydrology to an alkaline lake with more frequent basin restrictions.

Keywords: Re-Os geochronology, oil shale, biomarkers, Green River Formation

1. Introduction

Rhenium-osmium (Re-Os) geochronology of lacustrine organic-rich mudstones has been shown to yield age determinations that are consistent with $^{40}Ar/^{39}Ar$ ages of interbedded volcanic tuffs and biostratigraphic control (e.g., Cumming et al., 2012; Xu et al., 2017; Pietras et al., 2020). However, the uncertainty of these ages ranges widely. Uncertainties using the Re-Os isochron approach, beyond the level of analytical uncertainty, are controlled by the range of initial $^{187}Os/^{188}Os$ and $^{187}Re/^{188}Os$ values in the sample set, the number of samples, and the decay constant uncertainty. Although weathering and hydrothermal alteration can lead to inaccurate and imprecise results (Peucker-Ehrenbrink and Hannigan, 2000; Jaffe et al., 2002; Kendall et al., 2009a; Georgiev et al., 2012; Rooney et al., 2012), careful sample collection can limit their effects. Variability in initial $^{187}Os/^{188}Os$ ratios violates the assumption that all samples had the same value at the time of deposition (Davies et al., 2018; Toma et al., 2020). Sampling over a narrow stratigraphic range may minimize this variance (Selby and Creaser, 2005; Kendall et al., 2009b; Stein and Hannah, 2014; Rooney et al., 2015; Rooney et al., 2020); however, variability at the scale of centimeters may not be avoidable (Pietras et al., 2020). Further, a narrow range of $^{187}Re/^{188}Os$ values in the sample set can yield a poorly constrained isochron (e.g., Kendall et al., 2009b; Selby et al., 2009). This ratio is directly proportional to the Re/Os ratio in a sample, and thus a set of samples with a broad range of Re/Os ratios will yield an isochron with less uncertainty than a set of samples with a narrow range, all other constraints being consistent. What controls the Re/Os ratio in organic-rich mudstones is an important question to address.

In a study of the marine Devonian-Mississippian Woodford Shale, a relation between organic matter type and Re and Os concentrations was proposed based on the observation that samples with greater amounts of terrestrial organic matter possessed higher Re concentrations, but similar

Os concentrations compared to samples with predominately marine organic matter (Harris et al., 2013). Devonian marine shales in New York State also show a positive correlation between organic matter diversity and Re and Os fractionation (Liu et al., 2020). In a controlled culture study of modern macroalgae, various parts of the same specimen accumulated different concentrations of Re and Os by factors of over 6 and 2, respectively (Racionero-Gómez et al., 2016; Racionero-Gómez et al., 2017). Finally, in a study of the lacustrine Green River Formation in the Uinta Basin Re concentrations of samples from the Mahogany zone were less varied than those from the Douglas Creek Member (Cumming et al., 2012). This yielded a narrower range of $^{187}Re/^{188}Os$ ratios for the Mahogany zone and isochron ages and Os_i estimates with higher uncertainties. Based on kerogen typing, it was postulated that less organic matter diversity in the Mahogany zone led to the narrower range of $^{187}Re/^{188}Os$ ratios (Cumming et al., 2012).

Taken together, these previous studies suggest that organic matter type provides a primary control on the Re/Os ratio of a sample because each type chelates a different amount of Re and Os prior to burial. More specifically, it is expected that a set of samples from an organic-rich mudstone that contains a large diversity of organic matter should yield a broader range of $^{187}Re/^{188}Os$ ratios than a mudstone with low diversity because each sample would be more likely to have a unique mixture of organic matter. This study specifically investigates the relation between organic matter diversity, the range of $^{187}Re/^{188}Os$ ratios, and Re-Os age uncertainties of lacustrine organic-rich mudstones using kerogen typing and extractable organic matter biomarker analysis in combination with Re-Os isotope and concentration measurements. Samples were collected from the Green River Formation deposited in the Uinta Basin of Utah and Colorado across a transition from fresher water lacustrine deposits to more alkaline and saline units that should correspond to a shift from a cosmopolitan to a more restricted fauna, respectively.

2. Geologic Setting

2.1. Green River Formation in the Uinta Basin

The Uinta Basin (Figure 1) is one in a series of depressions formed during the Late Cretaceous through Eocene Laramide orogeny that subdivided the Sevier foreland with basement cored uplifts yielding localized flexural subsidence and ponding of sediment and water (Dickinson et al., 1988; Johnson, 1985). Lacustrine deposition began in the western part of the basin in latest Cretaceous time, expanding over much of the basin by the late Paleocene (Remy, 1992; Smith et al., 2008; Birgenheier et al. 2020; and references therein). Deposition of the lower part of the Green River Formation began in the Eocene with fluvio-lacustrine siliciclastic and carbonate facies that overlie and are laterally equivalent to the alluvial Wasatch Formation. In the eastern Uinta Basin, the middle part of the Green River Formation is composed of the Douglas Creek Member and lower part of the Parachute Creek Member. These are overlain by the Mahogany zone which marks the base of the upper part of the Green River Formation (Birgenheier et al. 2020). This study focuses on samples collected from the Douglas Creek Member, the lower Parachute Creek Member, and the Mahogany zone of the Eocene Green River Formation in three cores located near the eastern margin of the Uinta Basin (Figure 1C).

2.2. Douglas Creek Member

The Douglas Creek Member in the eastern Uinta Basin varies in thickness from about 65 to 610 meters and consists of sandstone, siltstone, mudstone, and oolitic, algal, and ostracodal

limestones (Cashion, 1967). It complexly interfingers with the Wasatch Formation to the south and correlates to the Sunnyside Delta interval in the western part of the basin (Johnson et al., 2017; Birgenheier et al., 2020). Siliciclastic-dominated units include highly seasonal semi-arid fluvial sandstones, floodplain mudstones, and deltaic sandstone and siltstone beds. Carbonate-dominated intervals indicate periods of more stable river discharge leading to persistent lacustrine depositional environments that allowed for the accumulation of organic-rich lacustrine mudstones, sublittoral carbonate mudstones, littoral to sublittoral carbonate grainstones and wackestones, and microbialites. Overall, the Douglas Creek Member is interpreted to have been deposited in a shallow low-gradient lake (Rosenberg et al., 2015; Birgenheier et al., 2020). The presence of microbialites and the absence of a freshwater molluscan assemblage, which is present in underlying deposits (Birgenheier et al., 2020), indicates increasing alkalinity and salinity.

2.3. Lower part of the Parachute Creek Member

The lower part of the Parachute Creek Member contrasts from the underlying Douglas Creek Member in the study area by an overall decrease in sandstone and increase in organic-rich mudstone beds termed oil shale (Johnson et al., 2010; Birgenheier and Vanden Berg, 2011). It also contains a repetitive stacking of lithofacies that are interpreted to represent lake expansion-contraction cycles. In these cycles oil shales were deposited during periods of relatively high lake level while desiccation cracks, wavey bedding, microbialites, and rip-up clasts represent lower lake levels and transgressive events (Brembs, 2017). They are typically 1-5 meters thick and their boundaries, which represent timelines, can be correlated for several kilometers

(Brembs, 2017). Chronostratigraphic correlations are further aided by numerous interbedded volcanic ash layers. Lake expansion-contraction cycles stack into larger scale zones that are on the order of several meters to about 40 meters thick (Figure 1A). These zones alternate from being more calcareous and organic-rich (R) to siliciclastic and organic-lean (L) (Birgenheier et al., 2020). They have been correlated within the Uinta Basin and eastward into the Piceance Creek Basin (Figure 1C) based on lithology, Fischer assay oil yields, and well log signatures (Donnell and Blair, 1970; Cashion and Donnell, 1972; Johnson, 1989; Birgenheier and Vanden Berg, 2011).

The lake expansion-contraction cycles in the lower Parachute Creek Member record frequent lake level oscillations below the elevation of the outflow sill (c.f. Carroll and Bohacs, 1999) and are similar to those recognized in the Green River Formation in the Greater Green River Basin in Wyoming (Eugster and Hardie 1975; Smoot, 1983; Rhodes et al., 2002; Pietras and Carroll, 2006). These cycles are not as well developed in the underlying Douglas Creek Member signifying a shift to a balanced fill hydrology from a more open hydrology across this boundary. The lack of evaporite deposits and a robust fossil fish assemblage in the lower Parachute Creek Member indicate that the basin did occasionally flush dissolved solutes over the sill during periods of high lake level.

2.4. Mahogany zone

The Mahogany zone is typically about 30 meters thick in the eastern Uinta Basin (Johnson et al., 2010) but reaches nearly 50 meters in some places. It is the most organic-rich interval in the study area with Fischer assay oil yields ranging from 10-30 gallons per ton or roughly 5-15%

total organic carbon (TOC), locally exceeding 70 gallons of oil per ton (Johnson et al., 2010; Birgenheier and Vanden Berg, 2011; Birdwell et al., 2015). It is primarily composed of massive to laminated, locally brecciated kerogen-rich mudstone with very few fish fossils deposited in a profundal setting below wave base in a density stratified lake (Birgenheier et al., 2020). Lake level was likely relatively stable during deposition of the Mahogany zone, in contrast to the underlying lower Parachute Creek Member, leading to the paucity of other facies, though mineral composition and organic richness have been shown to vary at the lamina scale (Washburn et al., 2016). Nahcolite nodules are present in the Mahogany zone in the Coyote Wash #1 core, and bedded nahcolite occurs in cores located closer to the basin depocenter (Birgenheier and Vanden Berg, 2011). The increase in organic richness, decrease in fish fossils, and presence of evaporative minerals is indicative of hydrologic closure which led to increased salinity, density stratification, and long term anoxic bottom waters prior to the main saline phase in the basin recorded by the overlying strata of the upper Green River Formation (Smith et al., 2008; Birgenheier et al., 2020).

3. Materials and methods

3.1. Samples

The Douglas Creek Member was originally sampled by Cumming et al. (2012) for Re-Os isotope analysis, programmed pyrolysis (e.g., Rock-Eval), and TOC in an anomalously thick (~3 meters) organic-rich layer that occurs about 115 meters below the top of the member in the Coyote Wash #1 core (Figure 1; 40° 1' 22.2240" N, 109° 18' 38.4834" W). This core is stored at the USGS Core Research Center in Denver, Colorado. The base of the Douglas Creek Member

was not penetrated in the Coyote Wash #1 core; however, regional correlations indicate that the sampled interval corresponds to roughly the middle of the Douglas Creek Member in one of the carbonate-dominated lacustrine zones (Birgenheier et al., 2020). This interval is primarily composed of massive to laminated kerogen-rich mudstone that was deposited under profundal to sublittoral conditions. Four intervals that were analyzed by Cumming et al. (2012) were resampled from the core for extractable organic matter (EOM) biomarker analysis (*n*-alkanes, acyclic isoprenoids, and β-carotane) using chloroform-soluble EOM (unfractionated).

Forty samples were collected from correlative oil shale beds in the R3 and R6 zones of the lower Parachute Creek Member in the Skyline 16 (39° 52′ 14.4336″ N, 109° 06′ 44.1678″ W) and PR15-7c (39° 59′ 26.6424″ N, 109° 00′ 59.4760″ W) cores (Figure 1). These cores are stored at the Utah Core Research Center in Salt Lake City, Utah. Ten samples were collected over an interval of 50 to 100 cm in each oil shale zone in each core. Chronostratigraphic corrections were based on decameter-scale organic-rich and organic-lean zones, meter-scale lake expansion and contraction cycles, volcanic ash layers, and distinct marker beds (Dennett, 2019). These samples were analyzed for Re-Os isotopes, programmed pyrolysis, and TOC. A subset of four samples from each oil shale bed in each core were also used for EOM biomarker analysis. Ten samples from Skyline 16 core and 2 from the PR15-7c core of an oil shale bed in the R4 zone of the lower Parachute Creek Member (Figure 1), originally analyzed for Re-Os isotopes (Pietras et al., 2020), were analyzed for programmed pyrolysis and TOC measurements. Four of these samples from the Skyline 16 core were also collected for EOM biomarker analysis. The R4 oil shale lies just above the Skyline ash (Figure 1A).

Four samples from the Mahogany zone in the Coyote Wash #1 core were collected for EOM biomarker analysis. These new samples coincide with those of Cumming et al. (2012) which

were analyzed for Re-Os isotopes, programmed pyrolysis, and TOC, and lie between the Curly and Wavy tuffs (Figure 1A).

3.1. Re-Os isotopic analysis

Samples were visually inspected to avoid diagenetic fracture fills, broken down by hand in a porcelain mortar and pestle, and then powdered and homogenized in an alumina ceramic ball mill. The Re-Os analyses were conducted at the Durham Geochemistry Centre at Durham University using the same standard procedures for organic-rich sedimentary rocks used by Cumming et al. (2012) and Pietras et al. (2020). Twenty to 40 grams of material from each sample were powdered, from which ~1 gram was used for Re-Os isotope analysis. The Re-Os analysis utilizes carius tube digestion to homogenize sample and tracer solution (spike), then solvent extraction, microdistillation, and chromatography methods to isolate and purify the Re and Os fractions (Shirley and Walker, 1995; Cohen and Waters, 1996; Birck et al., 1997; Selby and Creaser, 2003; Kendall et al., 2004; Cumming et al., 2013). In brief, about 1 gram of sample, plus a known amount of spike solution (^{190}Os + ^{185}Re) together with 8 mL of Cr^{VI}–H_2SO_4 solution (used to limit the incorporation of detrital Re and Os) were digested in a sealed carius tube for 48 hours at 220°C (Selby and Creaser, 2003; Kendall et al., 2004). The Os was purified using solvent extraction (chloroform, $CHCl_3$), and Cr^{VI}–H_2SO_4 – HBr micro-distillation. Rhenium was isolated and further purified using NaOH-acetone solvent extraction and anion chromatography. The purified Re and Os fractions were loaded onto Ni and Pt filaments, respectively (Selby, 2007). Isotopic measurements were performed using a ThermoScientific TRITON mass spectrometer via static Faraday collection for Re and ion-counting using a secondary electron multiplier in peak-hopping mode for Os. Total procedural

blanks during this study were 13.2 ± 0.4 pg and 0.06 ± 0.03 pg for Re and Os, respectively, with an average $^{187}Os/^{188}Os$ value of 0.21 ± 0.04 (n = 4). To monitor the long-term reproducibility of mass spectrometer measurements, two in-house Re and Os (DROsS) solution standards were analyzed, which yielded an average $^{185}Re/^{187}Re$ and $^{187}Os/^{188}Os$ ratio of 0.59862 ± 0.0008 and 0.16089 ± 0.00062 (1σ, n = 10) respectively during this study.

Uncertainties for $^{187}Re/^{188}Os$ and $^{187}Os/^{188}Os$ were determined by full error propagation of uncertainties in Re and Os mass spectrometer measurements, blank abundances and isotopic compositions, spike calibrations and reproducibility of standard Re and Os isotopic values. The Re-Os isotopic data including 2σ uncertainties for $^{187}Re/^{188}Os$ and $^{187}Os/^{188}Os$ and the associated error correlation function (rho) were regressed to yield Re-Os ages and Os_i values using *Isoplot v. 4.15* and *IsoplotR* with the λ ^{187}Re constant of 1.666×10^{-11} yrs^{-1} $\pm 5.165 \times 10^{-14}$ yrs^{-1} (Ludwig, 1980; Smoliar et al., 1996; Ludwig, 2012; Vermeesch, 2018). To account for deviation from the isochron, *Isoplot v. 4.15* assumes normally distributed variation in initial $^{187}Os/^{188}Os$ values (Ludwig, 2012) whereas *IsoplotR* assumes a non-normal variation (Vermeesch, 2018) that tends to yield more precise Re-Os ages.

3.2. Programmed Pyrolysis and TOC

Programmed pyrolysis and TOC measurements were conducted at the USGS Petroleum Geochemistry Research Laboratories (PGRL) in Denver, Colorado. For programmed pyrolysis, the amount of hydrocarbon (HC) products and oxygen bearing compounds (CO, CO_2) were measured to determine S_1 (mg-HC/g-rock, free oil), S_2 (mg-HC/g-rock, kerogen), S_3 (mg-CO_2/g-rock), and T_{max} (°C, pyrolysis temperature at maximum of the S2 peak). Crushed samples were

placed into a Wildcat Technologies Hydrocarbon Analyzer with Kinetics (HAWK), heated initially to 300°C and held for 3 minutes to measure S_1, then incrementally heated to 650°C (25°C/min, 14 minutes) to obtain S_3, followed by a cooling step between samples according to manufacturer's instructions. Both S_1 and S_2 measurements were made using a flame ionization detector (FID), whereas the S_3 parameter was determined by measuring CO_2 evolved up to 390°C using an infrared detector. TOC was measured using a LECO C744 Carbon Analyzer following the manufacturer's instructions (Dreier and Warden, 2021). Samples were acidified with 6 M HCl and rinsed with deionized water prior to combustion to remove inorganic carbon (carbonate). Quality control materials, including blanks, geochemical reference materials, and manufacturer's calibration standards, were analyzed during the analytical period for both methods. TOC uncertainty is 0.06 wt.% (2σ) based on the analysis of 10 standards. Six duplicate samples, 2 from each zone, were also analyzed for TOC and yield a reproducibility of 0.22 wt.% (2σ). The two data sets were combined to calculate the hydrogen index (HI = 100×S2/TOC) and oxygen index (OI = 100×S3/TOC) for each sample. These values were then plotted on a pseudo-Van Krevelen diagram to assess kerogen type (Espitalie et al., 1977; Peters, 1986). For information on anticipated variance in programmed pyrolysis samples, see Birdwell and Wilson (2019).

3.3. Biomarker analysis

A subset of core samples was Soxhlet-extracted with chloroform for ~48 hours to obtain EOM for biomarker characterization at USGS PGRL (Lowry, 2020a). Copper strips were cleaned with chloroform then added to round bottom flasks to remove elemental sulfur during the extraction process. After extraction, EOM samples were filtered and concentrated using a

vacuum rotary evaporator. To estimate the total mass of EOM removed from each rock sample, a known volume of the dissolved EOM was dried and weighed. Unfractionated EOM samples were analyzed by gas chromatography with a flame ionization detector (GC-FID) using an Agilent 6890 (see Lowry, 2020b for details). Using measured peak heights for selected *n*-alkanes, acyclic isoprenoids, and β-carotane, several biomarker parameters were calculated, including the carbon preference index (CPI; Marzi et al., 1993), pristane/phytane ratio (Pr/Ph), terrigenous/aquatic ratio (TAR; Bourbonniere and Meyers, 1996) and β-carotane/*n*-C_{30}. These parameters can provide insights into organic matter sources and depositional conditions in aquatic environments and have been used to differentiate lake basin type and organic matter source diversity in the Green River Formation and other lacustrine strata (Collister et al., 1994; Katz, 1995; Carroll and Bohacs, 2001; Peters et al., 2005).

4. Results

4.1. Re-Os

Elemental concentrations of Re and Os (^{192}Os) range from 11.3 to 32.7 ppb and 127.8 (42.3) to 300.1 (100.6) ppt, respectively for samples from the R3 and R6 zones (Table 1). These are similar to those reported from the underlying Douglas Creek Member, interbedded R4 zone, and overlying Mahogany zone (Cumming et al., 2012; Pietras et al., 2020). Samples from the R3 zone in the Skyline 16 core have a ^{187}Re/^{188}Os range of 434.5 to 865.9, a ^{187}Os/^{188}Os range of 1.755 to 2.118, and yield a Model 3 isochron age of 50.5 ±3.4 Ma (2σ) with a MSWD of 6.1 and an Os_i value of 1.39 ±0.04 (2σ) using *Isoplot v. 4.15* (Figure 2A). Samples from the R3 zone in the PR15-7c core have a ^{187}Re/^{188}Os range of 507.3 to 873.6, a ^{187}Os/^{188}Os range of 1.833 to

296 2.142, and yield a Model 3 isochron age of 47.2 ±7.6 Ma (2σ) with a MSWD of 16 and an Os_i
297 value of 1.44 ±0.09 (2σ) using *Isoplot v. 4.15* (Figure 2B). Combining samples from these
298 correlative cores yields a Model 3 isochron age of 49.7 ±3.4 Ma (2σ) with a MSWD of 10.7 for
299 the R3 zone and an Os_i value of 1.40 ±0.04 (2σ) with an Os_i variation of 0.034 (2σ) using *Isoplot*
300 *v. 4.15* (Figure 2C). The combined dataset yields a similar Model 3 isochron age of 49.7 ±3.0 Ma
301 (2σ) and an Os_i value of 1.40 ±0.03 (2σ) with an Os_i variation of 0.0318 +0.0073 / -0.0045 (2σ)
302 using *IsoplotR*.

303 Samples from the R6 zone in the Skyline 16 core have a $^{187}Re/^{188}Os$ range of 415.7 to 567.6, a
304 $^{187}Os/^{188}Os$ range of 1.751 to 1.918, and yield a Model 3 isochron age of 52.0 ±27 Ma (2σ) with
305 a MSWD of 35 and an Os_i value of 1.43 ±0.22 (2σ) using *Isoplot v. 4.15* (Figure 2D). Samples
306 from the R6 zone in the PR15-7c core have a $^{187}Re/^{188}Os$ range of 385.2 to 640.1, a $^{187}Os/^{188}Os$
307 range of 1.7691 to 1.962, and yield a Model 3 isochron age of 37.0 ±27 Ma (2σ) with a MSWD
308 of 50 and an Os_i value of 1.58 ±0.22 (2σ) using *Isoplot v. 4.15* (Figure 2E). Combining samples
309 from these correlative cores yields a Model 3 isochron age of 42.0 ±18 Ma (2σ) with a MSWD of
310 50 for the R6 zone and an Os_i value of 1.52 ±0.15 (2σ) with an Os_i variation of 0.072 (2σ) using
311 *Isoplot v. 4.15* (Figure 2F). The combined dataset yields a similar Model 3 isochron age of 42.3
312 ±16.4 Ma (2σ) and an Os_i value of 1.52 ±0.14 (2σ) with an Os_i variation of 0.0678 +0.0143 / -
313 0.0085 (2σ) using *IsoplotR*.

314 An Os_i estimate for each sample from the R3 and R6 zones was calculated using the ^{187}Re
315 decay constant of 1.666×10^{-11} per year (Smoliar et al., 1996) and a depositional age of 49 Ma
316 (Table 1). Analytical uncertainty was fully propagated using the square root of the sum of
317 squares approach and includes the uncertainty of the measured $^{187}Re/^{188}Os$ and $^{187}Os/^{188}Os$ ratios
318 and the 0.35% uncertainty of the ^{187}Re decay constant (Smoliar et al., 1996). An Os_i value was

calculated for the samples from Douglas Creek and Mahogany zones of Cumming et al. (2012) and the R4 zone of Pietras et al. (2020) using the same methodology (Table 2). The depositional age of 49 Ma was chosen because it lies near the midpoint of all Green River Formation samples examined here. Sensitivity analysis using 48 Ma and 50 Ma alters the Os_i calculations by ±0.02 at most. However, these results were only used to investigate the relative range of Os_i values in each set of samples, not to compare absolute Os_i values.

4.2. Total Organic Carbon & Programmed Pyrolysis

The TOC values for samples of the R3, R4, and R6 zones of the Parachute Creek Member in the Skyline 16 and PR15-7c cores range from 2.05 to 10.03 wt.% with an average of 5.63 wt.% (Table 3). The average TOC increases upwards from 4.67 wt.% in the R3 zone to 5.40 wt.% in the R4 zone and 6.73 wt.% in the R6 zone. These are lower than measurements in the Coyote Wash #1 core from the Douglas Creek Member and Mahogany zone with averages of 9.79 and 17.0 wt.%, respectively (Cumming et al., 2012).

Combining TOC measurements with parameters determined by programmed pyrolysis yields HI and OI values (Table 2) indicative of Type I algal oil-prone kerogen when plotted on a pseudo-Van Krevelen diagram (Figure 3A), as expected (Tissott and Welte, 1984; Caroll and Bohacs, 2001; and references therein). Samples from the Douglas Creek Member and Mahogany zone (Cumming et al., 2012) plot in a similar location, with the Douglas Creak Member samples defining a slightly broader OI range (Figure 3A). Samples from the R3, R4, and R6 zones have a production index (PI) of less than 0.07 with an average of 0.03 (Table 3), indicative of immature source rocks. This is consistent with samples from the Douglas Creek Member and Mahogany

zone (Cumming et al., 2012). A cross-plot of T_{max} versus Hydrogen Index (HI) also indicates that all samples are immature Type I source rocks (Figure 3B). Kinetic modeling suggests that the onset of the oil window for lacustrine source rocks is 120°C (range of 20°C) at a heating rate of 2°C Ma (Pepper and Corvi, 1995). Given that the average PI is below 0.10, the maximum burial temperature was likely well below 120°C for all samples used in this study.

4.3. EOM Biomarkers

The carbon preference index (CPI) has been widely used to assess the influence of terrigenous organic matter in organic-rich sedimentary rocks with higher values indicating a larger contribution of terrigenous inputs (Bray and Evans, 1961; Marzi et al., 1993; Peters et al., 2005). In the Green River Formation, Lillis et al. (2003) used CPI to aid in differentiating oil types, noting that the most common oils (type "A") were likely derived from units below the Douglas Creek Member in the lower Green River and have CPI values less than 1.1. Rarer Green River Formation oils (type "B") have CPI values greater than 1.2 and are sourced from the Mahogany zone and similar oil shale facies. In the EOM samples examined here, average CPI values increase from 1.18 in the Douglas Creek Member to 1.70 in R3 zone and 1.67 in R4 zone, reach a maximum of 2.31 in R6 zone, and then drop to 1.68 in the Mahogany zone (Table 4).

The terrigenous-aquatic ratio (TAR) has also been used in modern lacustrine and ancient marine settings to estimate the relative contribution of terrigenous organic matter, with values greater than 1 interpreted to indicate the presence of terrestrial organic matter in sedimentary EOM (Silliman et al., 1996; Bourbonniere and Meyers, 1996; French et al., 2019). Samples from the Douglas Creek Member have the lowest average TAR value of 0.90, while samples from the

R6 zone have the highest average TAR value of 4.16 (Table 4). Samples from the R3, R4, and the Mahogany zones have averages ranging from 2.2 to 3.06.

In immature source rocks, the ratio of the isoprenoids pristane and phytane (Pr/Ph) can be used to provide information on redox conditions (Peters et al., 2005), with values less than 1 indicating reducing-anoxic conditions. The most abundant source of pristane and phytane is the phytyl side chain of chlorophyll a in phototrophic organisms and bacteriochlorophyll a and b in purple sulfur bacteria (Brooks et al., 1969; Powell and McKirdy, 1973). Under reducing conditions phytol is converted to phytane, while under oxic conditions it is converted to pristane. However, organic matter source can also affect the ratio, with a Pr/Ph value greater than 3 indicating a significant contribution of terrigenous organic matter (Peters et al., 2005). Samples from the Douglas Creek Member have the highest average Pr/Ph ratio of 1.08 (Table 4). The average Pr/Ph ratio decreases up-section in the lower Parachute Creek Member from 0.42 in the R3 and R4 zones to 0.37 in the R6 zone. Samples from the Mahogany zone have an average Pr/Ph ratio of 0.64.

The compound β-carotane can also provide information on lacustrine depositional conditions, with high values (relative to various *n*-alkanes like *n*-C_{30}) generally interpreted as indicating highly reducing, anoxic-saline conditions, where halotolerant organisms produce β-carotene to prevent photoinhibition (Moldowan et al., 1985; Jiang and Fowler, 1986; Ben-Amotz et al., 1989; Fu et al., 1990; Irwin and Meyer, 1990; Peters et al., 2005). Samples from the Douglas Creek Member have the lowest average β-carotane/*n*-C_{30} ratio of 0.25 while values systematically increase from 0.96 to 2.32 to 5.29 in the R3, R4, and R6 zones, respectively (Table 4). Samples from the Mahogany zone have an average β-carotane/*n*-C_{30} ratio of 3.24.

5. Discussion

5.1. Re-Os Geochronology

The stratigraphic positions of the R3, R4, and R6 oil shales were projected onto the Coyote Wash #1 core based on correlation of organic-rich and lean zones in the lower Parachute Creek Member (Birgenheier and Vanden Berg, 2011). This allows for a direct comparison to the results of Cumming et al. (2012) from the Douglas Creek Member and Mahogany zone. Although all five Re-Os age determinations are statistically indistinguishable based on 2σ uncertainties, their mean ages fall in stratigraphic order, except for the age of the R6 oil shale (Figure 1B). They are also statistically indistinguishable from age determinations of interbedded volcanic ash beds based on $^{40}Ar/^{39}Ar$ geochronology (Smith and Carroll, 2015; and references therein). Examining the isochron for the combined R6 dataset, there are four samples that contribute to the large uncertainty (Figure 2F). Two have anomalously high $^{187}Os/^{188}Os$ ratios (P6-3, P6-7), and two have anomalously low $^{187}Os/^{188}Os$ ratios (S6-7, S6-10). As a test on their contribution to uncertainty these samples were removed to create a new Model 3 isochron for the R6 zone which yielded an age of 47.7 ±7.9 Ma (2σ) with a MSWD of 7.1 and an Os_i value of 1.48 ±0.07 (2σ) using *Isoplot v. 4.15* (Figure 4). The Os_i variation was reduced from 0.072 to 0.025 (2σ) when removing these four samples. Calculations using *IsoplotR* yielded an isochron age of 47.7 ±6.7 Ma (2σ) with an Os_i value of 1.48 ±0.06 (2σ). The Os_i variation was reduced from 0.0678 +0.0143 / -0.0085 (2σ) to 0.023 +0.0065 / -0.0038 (2σ). This mean age is more consistent with the results from the other four zones (Figure 1) but is statistically indistinguishable to the age determined using all 20 samples (Figure 4).

As a further assessment of the relative chronostratigraphic position of the five Re-Os age determinations, an average sedimentation rate was calculated (Figure 5). A simple linear regression through all 5 ages plotted versus their stratigraphic position in the Coyote Wash #1 core yields a sedimentation rate of 10.7 cm/kyr. While the sedimentation rate is not expected to have been linear given the variability in depositional environments, erosional events, or hiatuses, this average estimate is comparable to those calculated for members of the Green River Formation in Wyoming (16.95 cm/kyr; Meyers, 2008) and Colorado (15.20 cm/kyr; Dyer-Pietras, 2020) based on the average spectral misfit approach and stratigraphic thicknesses between volcanic ashes with known $^{40}Ar/^{39}Ar$ ages (8.5 cm/kyr for the Tipton Shale Member, 22.5 cm/kyr for the Wilkins Peak Member, and 11 cm/kyr for the Laney Member; Pietras and Carrol, 2003). Although the uncertainty on these ages is quite large; taken together, their combined ages appear to be robust. This again further highlights the utility of Re-Os geochronology of organic-rich mudstones in lacustrine and marine basins. This is particularly true in thick successions that lack volcanic ash layers, reliable biostratigraphy, or magnetostratigraphic data where a few age determinations, even those with large uncertainties, would be valuable to constrain burial history and thermal history models or allow for temporal correlation to the broader geological record (e.g., Lúcio et al., 2020; Rooney et al., 2020; Toma et al., 2020).

5.2. Os_i Stratigraphy

The initial $^{187}Os/^{188}Os$ ratios derived from isochrons of samples from the Douglas Creek Member, R3, R4, R6 and Mahogany zone show a bulk shift from a value of 1.40 to 1.48 between

the R3 and R4 zones with an associated shift in the range of the 2σ uncertainty bars (Figure 1B). Interestingly, this small isotopic transition occurs 20 to 50 meters above the contact between the Douglas Creek and the lower Parachute Creek members during a time when the basin transitioned from a more open hydrology to a more alkaline and saline lake with frequent basin restrictions. Thus, this shift may be related to changes in the chemical weathering products entering the lake (Peucker-Ehrenbrink and Ravizza, 2000; Lu et al., 2017) in the course of drainage basin evolution. Further study of the $^{187}Os/^{188}Os$ composition of bedrock surrounding the basin, along with additional sampled intervals is warranted to understand the long-term Os isotopic stratigraphy of the Uinta Basin and the role of drainage basin change. However, to our knowledge these five data points define the largest Os isotope stratigraphic record from any lacustrine basin compiled to date.

5.3. Re-Os Isochron Uncertainty

The uncertainty of Re-Os isochron age determinations and Os_i estimates using the isochron method is a function of analytical uncertainty, variance of initial $^{187}Os/^{188}Os$ values in the sample set, the range of $^{187}Re/^{188}Os$ values in the sample set, the number of samples, and decay constant uncertainty. To evaluate the relative contribution of these parameters on the age uncertainty for samples of the Green River Formation, a theoretical $^{187}Re/^{188}Os$ range of the sample set versus age uncertainty curve was developed (Figure 6). For this, isochron ages were determined using *Isoplot v. 4.15* with a set of 20 samples that had a total range of $^{187}Re/^{188}Os$ ratios varying from 50 to 1600. Samples were evenly spaced within each range, and the range was incrementally increased by 50 for a total of 32 isochrons. The present-day $^{187}Os/^{188}Os$ value for each sample

was calculated assuming an initial $^{187}Os/^{188}Os$ value of 1.40 and an age of 49 Ma, the approximate age of the Green River Formation samples. These assumptions remove Os_i variability from the sample set, and as a contributor to age uncertainty. Average analytical uncertainties (Table 5) for the $^{187}Re/^{188}Os$ ratio, $^{187}Os/^{188}Os$ ratio, and associated error correlation (rho) were determined using all Green River Formation samples (this study; Cumming et al., 2012; Pietras et al., 2020). A second curve (dashed line on Figure 6) was calculated using the same methodology with a set of 10 samples to highlight the impact of population size on age uncertainty. Sensitivity analysis using ages of 48 Ma and 50 Ma yielded results that are within the width of the lines on Figure 6.

Age uncertainties for all five zones of the Green River Formation lie above the theoretical curves (circles on Figure 6) indicating contributions from Os_i variance within each sample set or analytical uncertainties greater than the average of all samples. To determine the influence of these two parameters, a set of samples was generated for each zone with the same $^{187}Re/^{188}Os$ range and number of samples as the original set; however, the initial $^{187}Os/^{188}Os$ value for every sample was set to 1.40 and present-day $^{187}Os/^{188}Os$ values were calculated assuming a depositional age of 49 Ma as was done for the theoretical curves. However, the average analytical uncertainties for the $^{187}Re/^{188}Os$ ratio, $^{187}Os/^{188}Os$ ratio, and associated error correlation (rho) were calculated separately for each zone (Table 5). Age uncertainties calculated with *Isoplot v. 4.*15 using these local parameters for the R3, R4, and R6 zones lie below the theoretical curves (squares on Figure 6). Since these zones have analytical uncertainties that are comparable to those used for the theoretical curves (Table 5) it can be assumed that the actual age uncertainty for these zones, beyond what can be attributed to their range of $^{187}Re/^{188}Os$ values, is due to variance in Os_i values. In fact, samples from the R6 zone have the largest Os_i

variance of the three zones (Table 6) and the largest deviation from the theoretical curves (Figure 6). The age uncertainty calculated with *Isoplot v. 4.*15 using local parameters for the Douglas Creek Member lies very close to the theoretical curve curves (square on Figure 6) indicating that while average analytical uncertainties for the zone are high (Table 5), this appears to be mitigated by having a broad range of $^{187}Re/^{188}Os$ values (1504). The actual age uncertainty for the Douglas Creek Member is much higher (circle on Figure 6) and it is primarily controlled by the large variance in Os_i (Table 6). The $^{187}Os/^{188}Os$ ratio of lake water can vary at rates of 0.01 per kilo-year, perhaps two orders of magnitude faster than in open marine basins (Pietras et al., 2020). At this rate, even very high-resolution stratigraphic sampling from cores may not reduce Os_i variance in a set of samples due to the requirement of large sample sizes. Lateral sampling from a narrow stratigraphic interval (<2 centimeters) in outcrop may be required. In contrast to the Douglas Creek Member, samples from the Mahogany zone have the narrowest Os_i variance (Table 6), but the age uncertainty is well above the theoretical line (circle on Figure 7). This can be attributed to higher average analytical uncertainties for these samples (Table 5) which was not mitigated by a broad range of $^{187}Re/^{188}Os$ values, in fact the Mahogany zone has the narrowest $^{187}Re/^{188}Os$ values (154.6) of any zone studied.

While this analysis indicates unique controls on the age uncertainty for each zone of the Green River Formation, a more general observation is apparent. The theoretical curve indicates that sample sets with a $^{187}Re/^{188}Os$ range of less than about 500 have age uncertainties that are significantly higher than those with larger ranges (Figure 6). Samples from the Green River Formation follow this trend once Os_i variability and analytical uncertainty are accounted for, providing an opportunity to investigate the control on the $^{187}Re/^{188}Os$ range. It should be noted that each set of samples is unique and those with a $^{187}Re/^{188}Os$ range of less than 500 can yield

age determinations with a lower percentage of uncertainty than presented here (e.g., Rooney et al., Toma et al., 2020).

5.4. Re-Os Isochron Uncertainty and Organic Matter Diversity

Previous studies have suggested that organic matter type provides a primary control on the concentrations of Re and Os, and as a result the $^{187}Re/^{188}Os$ ratio, preserved in sedimentary organic matter (Cumming et al., 2012; Harris et al., 2013; Racionero-Gómez et al., 2017; Liu et al., 2020). It is expected that a sample set of organic-rich mudstone with a more diverse and varied assemblage of organic matter would yield a broader range of $^{187}Re/^{188}Os$ ratios because each sample would have a unique mixture of organic matter. To test this hypothesis kerogen type and EOM biomarker data were compared to the range of $^{187}Re/^{188}Os$ ratios from samples of the Green River Formation.

Samples from the R6 and Mahogany zones have the narrowest HI ranges of 170 and 155 mg HC/g TOC, respectively, as well as the highest average HI values of 964 and 1036 mg HC/g TOC, respectively (Figure 3B). Samples from the Douglas Creek Member, R3, and R4 zones define wider HI ranges of 237, 292, and 214 mg HC/g TOC, respectively and lower average HI values of 939, 889, and 905 mg HC/g TOC, respectively (Figure 3B). While all samples indicate the predominance of Type I, algal, oil-prone kerogen, those from the R6 and Mahogany zones define a slightly more homogenous kerogen type. The Douglas Creek Member contains samples with the highest OI values (Figure 3B) suggesting a contribution of Type III kerogen, typical of terrestrial plants. However, CPI and TAR values (Figure 7A) indicate less terrigenous organic

matter input during Douglas Creek Member deposition. Thus, the higher OI values may be due to oxidative degradation of organic matter by various metabolic processes.

Samples from the Douglas Creek Member have higher pristane/phytane ratios and very low β-carotane/n-C_{30} ratios (Figure 7B) indicative of deposition in an oxic-anoxic environment with low salinity that would have allowed for the accumulation of a diverse assemblage of aquatic organisms. Samples from the R3, R4, R6, and Mahogany zones all have lower pristane/phytane ratios and higher average β-carotane/n-C_{30} ratios than the Douglas Creek Member (Figure 7B) suggesting deposition in a more hydrologically restricted lacustrine environment with elevated salinities and alkalinities. This is consistent with sedimentological, stratigraphic, and paleontological evidence (Cashion, 1967; Rosenberg et al., 2015; Brembs, 2017; Birgenheier et al., 2020). For example, the occurrence of lake expansion-contraction cycles and a lack of evaporite deposits, except for the Mahogany zone, indicates deposition in a balanced-fill basin similar to the Laney Member of the Green River Formation in Wyoming which has a similar biomarker signature (Carroll and Bohacs, 2001). In detail, samples from the R6 and Mahogany zones appear to contain the least diverse aquatic organic matter assemblage based on narrowest HI ranges and highest β-carotane/n-C_{30} ratios with a slightly larger contribution, or better preservation, of terrigenous organic matter (Figure 7).

The trends in organic matter diversity suggested by kerogen type and EOM covary positively to the range of $^{187}Re/^{188}Os$ ratios from samples of the Green River Formation (Figure 7B). The Douglas Creek Member has the highest level of organic matter diversity and the largest range of $^{187}Re/^{188}Os$ ratios while the R6 and Mahogany zones have the lowest. The R3 and R4 zones have intermediate levels of organic matter diversity and $^{187}Re/^{188}Os$ ranges. Samples from the Green River Formation appear to confirm the hypothesis that organic matter diversity provides a

primary control on the range of $^{187}Re/^{188}Os$ ratios, and thus isochron uncertainties of organic-rich mudstones. Thus, it is expected that Re-Os geochronology of freshwater lacustrine organic-rich mudstones will more likely yield age determinations with lower uncertainties than those from saline lakes assuming a similar degree of Os_i variability and analytical uncertainty. Similarly, marine sediments with a cosmopolitan organic matter type provide a greater likelihood of yielding both age and Os_i determinations with higher precision than those with a restricted organic matter type.

6. Conclusions

Two new Re-Os age determinations of organic-rich lacustrine mudstones from the Green River Formation in the Uinta Basin were calculated. Although the uncertainty of these ages is quite large, the ages of the R3 zone (49.7 ±3.4 Ma) and R6 zone (42.0 ±18 Ma) are statistically indistinguishable from three previous Re-Os age determinations of organic-rich lacustrine mudstones and those based on $^{40}Ar/^{39}Ar$ geochronology of interbedded volcanic ash beds in the basin, highlighting the utility of Re-Os geochronology in lacustrine basins, particularly those that lack volcanic ash layers, reliable biostratigraphy, or magnetostratigraphic control. The five Re-Os ages fall in stratigraphic order, except for the R6 zone which has the largest uncertainty, and yield an average sedimentation rate of 10.7 cm/kyr which is comparable to those calculated for members of the Green River Formation in Wyoming. Initial $^{187}Os/^{188}Os$ ratios of the five sets of samples record a shift from a value of 1.40 to 1.48 between the R3 and R4 zones in the lower Parachute Creek Member. This indicates a change in the chemical weathering products entering the lake 20 to 50 meters above the contact between the Douglas Creek and the lower Parachute

Creek members during the time when the basin transitioned from a shallow freshwater lake with open hydrology to an alkaline lake with occasional basin restrictions (Birgenheier et al., 2020; and references therein).

The five Re-Os isochron determinations have relativity high and varied uncertainties, ranging from 5 to 43 % of the determined age. These high uncertainties, beyond the level of analytical uncertainty, are attributed to variability of Os_i and the range of $^{187}Re/^{188}Os$ values in the sample sets. Initial $^{187}Os/^{188}Os$ variability within individual organic-rich layers attests to the extreme sensitivity of the Os isotopic system in lacustrine basins.

The range of $^{187}Re/^{188}Os$ values of the five studied intervals generally correlates with the trends in organic matter diversity indicated by kerogen type and EOM biomarkers. The Douglas Creek Member was deposited during the period when the basin had the most open hydrology in the studied interval and records the highest degree of organic matter diversity and largest range of $^{187}Re/^{188}Os$ ratios. The R6 and Mahogany zones were deposited in a more most restricted basin with a lower diversity of organic matter and have the narrowest range of $^{187}Re/^{188}Os$ ratios. The R3 and R4 zones have intermediate levels of organic matter diversity and $^{187}Re/^{188}Os$ ranges. As noted in previous studies, the results of this study suggest that organic matter diversity plays a fundamental role on the range of $^{187}Re/^{188}Os$ ratios in a set of samples, that ultimately controls the level of uncertainty on Re-Os age determinations.

Acknowledgments

Acknowledgment is made to the Donors of the American Chemical Society Petroleum Research Fund (55391-DNI2) for support of this research (to JTP). We thank Michael Vanden Berg, Lauren Birgenheier, and the staff of the Utah Core Research Center at the Utah Geological

Survey for valuable geologic discussions, logistical support, and access to core samples. We also thank the U.S. Geological Survey (USGS) Core Research Center for sample access and the USGS Petroleum Geochemistry Research Laboratory for analytical support. DS is thankful for the ongoing support from Antonia Hofmann, Geoff Nowell, and Chris Ottley. Paul Lillis and Ronald Johnson provided insightful comments on an early version of this manuscript. Finally, we are grateful to David van Acken and an anonymous reviewer for their comments and suggestions.

References

Ben-Amotz, A., Shaish, A., and Avron, M., 1989, Mode of action of the massively accumulated beta-carotene of *Dunaliella bardawil* in protecting the alga against damage by excess irradiation: Plant Physiology, v. 91, p. 1040-1043.

Birck, J.L., Roy-Barman, M., and Capmas, F., 1997, Re-Os isotopic measurements at the femtomole level in natural samples: Geostandards Newsletter, v. 20, p. 19-27.

Birdwell, J.E., Mercier, T.J., Johnson, R.C., and Brownfield, M.E., 2015, In-place oil shale resources of the Mahogany zone sorted by grade, overburden thickness and stripping ratio, Green River Formation, Piceance Basin, Colorado and Uinta Basin, Utah: U.S. Geological Survey Fact Sheet 2015-3005.

Birdwell, J.E., Wilson, S.A., 2019, Variability in results from mineralogical and organic geochemical interlaboratory testing of USGS shale reference materials: Unconventional Resources Technology Conference, URTec 457.

Birgenheier, L.P., and Vanden Berg, M.D., 2011, Core-based integrated sedimentologic, stratigraphic, and geochemical analysis of the oil shale bearing Green River Formation,

609 Uinta Basin, Utah: Topical Report Submitted to the U.S. Department of Energy,
610 National Energy Technology Laboratory, DOE Award No. DE-FE0001243, Salt Lake
611 City, Utah, University of Utah, Institute for Clean and Secure Energy.
612 Birgenheier, L.P., Vanden Berg, M.D, Plink-Björklund, P., Gall, R.D., Rosencrans, E.,
613 Rosenberg, M.J., Toms, L.C., and Morris, J., 2020, Climate impact on fluvial-lake
614 system evolution, Eocene Green River Formation, Uinta Basin, Utah, USA: Geological
615 Society of America Bulletin, v. 132, p. 562-587.
616 Bourbonniere, R.A., and Meyers, P.A., 1996, Sedimentary geolipid records of historical
617 changes in the watersheds and productivities of Lakes Ontario and Erie: Limnology and
618 Oceanography, v. 41, p. 352-359.
619 Bray, E.E., and Evans, E.D., 1961, Distribution of *n*-paraffins as a clue to recognition of
620 source beds: Geochimica et Cosmochimica Acta, v. 22, p. 2-15.
621 Brembs, R.G, 2017, Cyclostratigraphy and chemostratigraphy in the Parachute Creek Member
622 of the Eocene Green River Formation, eastern Uinta Basin, Utah [MS Thesis]: Binghamton
623 University, State University of New York, Binghamton, New York, 246 p.
624 Brooks, J., Gould, K., and Smith, J., 1969, Isoprenoid hydrocarbons in coal and petroleum:
625 Nature, v. 222, p. 257-259.
626 Carroll, A.R., and Bohacs, K.M., 1999, Stratigraphic classification of ancient lakes: balancing
627 tectonic and climatic controls: Geology, v. 27, p. 99-102.
628 Carroll, A.R., and Bohacs, K.M., 2001, Lake-type controls on petroleum source rock
629 potential in nonmarine basins: AAPG Bulletin, v. 85, p. 1033-1053.

630 Cashion, W.B., 1967, Geology and fuel resources of the Green River Formation,
631 southeastern Uinta Basin, Utah and Colorado: U.S. Geological Survey Professional
632 Paper 548, 48p.
633 Cashion, W.B., and Donnell, J.R., 1972, Chart showing correlation of selected key units in
634 the organic-rich sequence of the Green River Formation, Piceance Creek Basin,
635 Colorado, and Uinta Basin, Utah: U.S. Geological Survey Oil and Gas Investigations
636 Chart OC-65.
637 Cohen, A.S., and Waters, F.G., 1996, Separation of osmium from geological materials by solvent
638 extraction for analysis by thermal ionization mass spectrometry: Analytica Chimica Acta, v.
639 332, p. 269-275.
640 Collister, J.W., Lightfouse, E., Hieshiam, G., and Hayes, J.M., 1994, Partial resolution of sources
641 of *n*-alkanes in the saline portion of the Parachute Creek Member, Green River Formation
642 (Piceance Creek Basin, Colorado): Organic Geochemistry, v. 21, p. 645-659.
643 Cumming, V.M., Selby, D., and Lillis, P.G., 2012, Re–Os geochronology of the lacustrine
644 Green River Formation: Insights into direct depositional dating of lacustrine successions,
645 Re-Os systematics and paleocontinental weathering: Earth and Planetary Science Letters, v.
646 359-360, p. 194-205.
647 Cumming, V.M., Poulton, S.W., Rooney, A.D., and Selby, D., 2013, Anoxia in the terrestrial
648 environment during the Late Mesoproterozoic: Geology, v. 41, p. 583-586.
649 Davies, J.H.F.L., Sheldrake, T.E., Reimink, J.R., Wotzlaw, J.F., Moeck, C., and Finlay, A., 2018,
650 Investigating complex isochron data using mixture models: Geochemistry, Geophysics,
651 Geosystems: v. 19, p. 4035-4047.
652 Dennett, A., 2019, Rhenium-osmium isotope systematics: applications of osmium isotope

stratigraphy and geochronology in lacustrine organic-rich mudstones of the Green River Formation, Eastern Uinta Basin, Utah [MS Thesis]: Binghamton University, State University of New York, Binghamton, New York, 128 p.

Donnell, J.R., and Blair, R.W., 1970, Resource appraisal of three rich oil-shale zones in the Green River Formation, Piceance Creek Basin, Colorado: Colorado School of Mines Quarterly, v. 65, p. 73–87.

Dickinson, W.R., Klute, M.A., Hayes, M.J., Janecke, S.U., Lundin, E.R., McKittrick, M.A., and Olivares, M.D., 1988, Paleogeographic and paleotectonic setting of Laramide sedimentary basins in the central Rocky Mountain region: Geological Society of America Bulletin, v. 100, p. 1023-1039.

Dreier, M., and Warden, A., 2021, Petroleum Geochemistry Research Laboratory Programmed Pyrolysis Method: U.S. Geological Survey Web Page, https://doi.org/10.5066/P9HQSBGH.

Dyer-Pietras, K.M., 2020, Insolation forcing of sub-lacustrine debris flows – Could monsoon intensification have played a role? Eocene lacustrine Green River Formation, Piceance Creek Basin, Colorado: Palaeogeography, Palaeoclimatology, Palaeoecology, v. 553.

Espitalié, J., Laporte, J.L., Madec, M., Marquis, F., Leplat, P., Paulet, J., and Boutefeu, A., 1977, Méthode rapide de caractérisation des roches mères, de leur potential pétrolier et de leur degré d'évolution: Revue Institut Français du Pétrole, v. 32, p. 23-42.

Eugster, H.P., and Hardie, L.A., 1975, Sedimentation in an ancient playa-lake complex: the Wilkins Peak Member of the Green River Formation of Wyoming: Geological Society of America Bulletin, v. 86, p. 319-334.

676 French, K.L., Birdwell, J.E., and Whidden, K.J., 2019, Geochemistry of immature Eagle
677 Ford Group drill core in East Texas: Organic Geochemistry, v. 131, p. 19-33.
678 Fu, J., Sheng, G., Xu, J., Eglington, G., Gowar, A.P., Jia, R., Fan, S., and Peng, P., 1990,
679 Application of biological markers in the assessment of paleoenvironments of Chinese
680 non-marine sediments: Organic Geochemistry, v. 16, p. 769-779.
681 Georgiev, S., Stein, H.J., Hannah, J.L. Weiss, H.M., Bingen, B., Guangping, X., Rein, E.,
682 Hatlø, V., Løseth, H., Nali, M., and Piasecki, S., 2012, Chemical signals for oxidative
683 weathering predict Re-Os isochroneity in black shales, East Greenland: Chemical
684 Geology, v. 324-325, p. 108-121.
685 Harris, N.B., Mnich, C.A., Selby, D., and Korn, D., 2013, Minor and trace element and Re-
686 Os chemistry of the Upper Devonian Woodford Shale, Permian Basin, west Texas:
687 Insights into metal abundance and basin processes: Chemical Geology, v. 356, p. 76-93.
688 Irwin, H., and Meyer, T., 1990, Lacustrine organic facies, a biomarker study using
689 multivariate statistical analysis: Organic Geochemistry, v. 16, p. 176-210.
690 Jaffe, L.A., Peuker-Ehrenbrink, B.P., and Petsch, S.T., 2002, Mobility of rhenium, platinum
691 group elements and organic carbon during black shale weathering: Earth and Planetary
692 Science Letters, v. 198, p. 339-353.
693 Jiang, Z., and Fowler, M.G., 1986, Carotenoid-derived alkanes in oils from northwestern
694 China: Organic Geochemistry, v. 10, p. 831-839.
695 Johnson, R.C., 1985, Early Cenozoic history of the Uinta and Piceance Creek basins, Utah
696 and Colorado, with special reference to the development of Eocene Lake Uinta, in
697 Flores, R.M., and Kaplan, S.S., eds., Cenozoic Paleogeography of the West-Central

United State, Rocky Mountain Section Symposium 3: Society for Economic Geologists and Paleontologists, p. 247-276.

Johnson, R.C., 1989, Detailed cross sections correlating Upper Cretaceous and Lower Tertiary rocks between the Uinta Basin of eastern Utah and western Colorado and the Piceance Basin of western Colorado: U.S. Geological Survey Miscellaneous Investigations Series Map I–1974, 2 sheets.

Johnson, R.C., Mercier, T.J., Brownfield, M.E., and Self, J.G., 2010, Assessment of in-place oil shale resources in the Eocene Green River Formation, Uinta Basin, Utah, and Colorado: U.S. Geological Survey Digital Data Series DDS–69–BB, Chapter 1, 153 p.

Johnson, R.C., Birdwell, J.E., and Lillis, P.G., 2017, Stratigraphic intervals for oil and tar sand deposits in the Uinta Basin, Utah: The Mountain Geologist, v. 54, p. 227-264.

Katz, B.J., 1995, The Green River Shale: An Eocene carbonate lacustrine source rock, *in* Katz, B.J., ed., Petroleum source rocks, Springer, Berlin, Heidelberg, p. 309-324.

Kendall, B.S., Creaser, R.A., Ross, G.M., and Selby, D., 2004, Constraints on the timing of Marinoan "Snowball Earth" glaciation by ^{187}Re-^{187}Os dating of a Neoproterozoic, post-glacial black shale in Western Canada: Earth and Planetary Science Letters, v. 222, 729-740.

Kendall, B., Creaser, R.A., Gordon, G.W. and Anbar, A.D., 2009a, Re-Os and Mo isotope systematics of black shales from the Middle Proterozoic Velkerri and Wollogorang Formations, McArthur Basin, northern Australia: Geochimica et Cosmochimica Acta, v. 73, p. 2534-2558.

Kendall, B., Creaser, R.A., and Selby, D., 2009b, ^{187}Re-^{187}Os geochronology of Precambrian organic-rich sedimentary rocks: Geological Society of London Special Publications 326, p.

721 85-107.
722 Lillis, P.G., Warden, A., and King, J.D., 2003, Petroleum systems of the Uinta and Piceance
723 basins: Geochemical characteristics of oil types: U.S. Geological Survey Digital Data
724 Series, DD-69-B, Chapter 3, 25p.
725 Liu, Z., Selby, D., Hackley, P.C., and Over, D.J., 2020, Evidence of wildfires and elevated
726 atmospheric oxygen at the Frasnian–Famennian boundary in New York (USA):
727 implications for the Late Devonian mass extinction: Geological Society of America
728 Bulletin, v. 132, p. 2043-2054.
729 Lowry, Z.K., 2020a. Petroleum Geochemistry Research Laboratory (PGRL) Method for
730 determining saturate, aromatic, resin, and asphaltene composition of rock extracts and
731 crude oil: U.S. Geological Survey Web Page, https://doi.org/10.5066/P901N4FH
732 Lowry, Z.K., 2020b. Petroleum Geochemistry Research Laboratory method for qualitative
733 analysis of crude oil and rock extracts by gas chromatography with flame ionization
734 detection, U.S. Geological Survey Web Page, https://doi.org/10.5066/P93XH0ZW
735 Lu, X., Kendall, B., Stein, H.J., and Hannah, J.L., 2017, Temporal record of osmium
736 concentrations and $^{187}Os/^{188}Os$ in organic-rich mudrocks: implications for the osmium
737 geochemical cycle and the use of osmium as a paleoceanographic tracer: Geochimica et
738 Cosmochimica Acta, v. 216, p. 221-241.
739 Lúcio, T., Souza Neto, J.A., Selby, D., 2020, Late Barremian / Early Aptian Re-Os age of the
740 Ipubi Formation black shales: stratigraphic and paleoenvironmental implications for
741 Araripe Basin, northeastern Brazil: Journal of South American Earth Sciences, v. 102., p.
742 102699.

743 Ludington, S., Moring, B.C., Miller, R.J., Stone, P.A., Bookstrom, A.A., Bedford, R.T., Evans,
744 J.G., Haxel, G.A., Nutt, C.J., Flyn, K.S., and Hopkins, M.J., 2005, Preliminary integrated
745 geologic map databases for the United States - western states: California, Nevada, Arizona,
746 Washington, Oregon, Idaho, and Utah: U.S. Geological Survey Open-File Report 2005-1305.
747 Ludwig, K.R., 1980, Calculation of uncertainties of U-Pb isotope data: Earth and Planetary
748 Science Letters, v. 46, p. 212-220.
749 Ludwig, K.R., 2012, Isoplot version 3.75: A geochronological toolkit for microsoft Excel:
750 Berkeley Geochronology Center Special Publication No. 5, 75 p.
751 Marzi, R., Torkelson, B.E., and Olson, R.K., 1993, A revised carbon preference index: Organic
752 Geochemistry, v. 20, p. 1303-1306.
753 Meyers, S.R., 2008, Resolving Milankovitchian controversies: The Triassic Latemar Limestone
754 and the Eocene Green River Formation: Geology, v. 36, p. 319-322.
755 Moldowan, J.M., Seifert, W.K., and Gallegos, E.J., 1985, Relationship between petroleum
756 composition and depositional environment of petroleum source rocks: American Association
757 of Petroleum Geologists Bulletin, v. 69, p. 1255-1268.
758 Pepper, A.S., and Corvi, P.J., 1995, Simple kinetic models of petroleum formation Part I: oil and
759 gas generation from kerogen: Marine and Petroleum Geology, v. 12, p. 291-319.
760 Peters, K.E., 1986, Guidelines for evaluating petroleum source rock using programmed
761 pyrolysis: AAPG Bulletin, v. 70, p. 318-329.
762 Peters, K., Walters, C., and Moldowan, J., 2005, The biomarker guide: biomarkers and isotopes
763 in petroleum exploration and earth history: United Kingdom, Cambridge University Press,
764 1155 p.

765 Peucker-Ehrenbirnk, B., and Hannigan, R.E., 2000, Effects of black shale weathering on the
766 mobility of rhenium and platinum group elements: Geology, v. 28, p. 475-478.
767 Peucker-Ehrenbirnk, B., and Ravizza, G., 2000, The marine osmium isotope record: Terra Nova,
768 v. 12, p. 205-219.
769 Pietras, J. T., and Carroll, A. R., 2003, Different lake types, same organic matter
770 accumulation rate: implications for carbon burial in the Eocene Green River Formation:
771 GSA Abstracts with Programs, v. 35, p. 104.
772 Pietras, J.T. and Carroll, A.R., 2006, High-resolution stratigraphy of an underfilled lake
773 basin: Wilkins Peak Member, Eocene Green River Formation, Wyoming, U.S.A.:
774 Journal of Sedimentary Research, v. 76, pp. 1197-1214.
775 Pietras, J.T., Selby, D., Brembs, R., and Dennett, A., 2020, Tracking drainage basin
776 evolution, continental tectonics, and climate change: implications from osmium isotopes
777 of lacustrine systems: Palaeogeography, Palaeoclimatology, Palaeoecology, v. 537.
778 Powell, T.G., and McKirdy, D.M., 1973, Relationship between ratio of pristane to phytane,
779 crude oil composition and geological environment in Australia: Nature Physical
780 Science, v. 243, p. 37-39
781 Racionero-Gómez, B., Sproson, A.D., Selby, D., Greenwell, H.C., Gröcke, D.R., Redden,
782 2016, Rhenium uptake and distribution in Phaeophyceae macroalgae, *Fucus*
783 *vesiculosus*: Royal Society Open Science, v. 3, 160161,
784 http://dx.doi.org/10.1098/rsos.160161.
785 Racionero-Gómez, B., Sproson, A.D., Selby, D., Gannoun, A., Gröcke, D.R., Greenwell,
786 H.C, and Burton, K.W., 2017, Osmium uptake, distribution, and $^{187}Os/^{188}Os$ and
787 $^{187}Re/^{188}Os$ compositions in Phaeophyceae macroalgae, *Fucus vesiculosus*: implications

for determining the $^{187}Os/^{188}Os$ composition of seawater: Geochimica et Cosmochimca Acta, v. 199, p. 48-57.

Remy, R., 1992, Stratigraphy of the Eocene part of the Green River formation in the south-central part of the Uinta Basin, Utah: U.S. Geological Survey Bulletin 1787-B, 79 p.

Rhodes, M.K., Carroll, A.R., Pietras, J.T., Beard, B.L., and Johnson, C.M., 2002, Strontium isotope record of paleohydrology and continental weathering, Eocene Green River Formation, Wyoming: Geology v. 30, p. 167-170.

Rooney, A.D, Selby, D., Lewan, M.D., Lillis, P.G., and Houzay, J-P., 2012, Evaluating Re-Os systematics in organic-rich sedimentary rocks in response to petroleum generation using hydrous pyrolysis experiments: Geochimica et Cosmochimica Acta, v. 77, p. 275-29.

Rooney, A.D., Strauss, J.V., Brandon, A.D., and Macdonald, F.A., 2015, A Cryogenian chronology: two long-lasting synchronous Neoproterozoic glaciations: Geology v. 43, p. 459-462.

Rooney, A.D., Cantine, M.D., Bergmann, K.D, Gómez-Pérez, I., Al Baloushi, B., Boag, T.H, Busch, J.F., Sperling, E.A., and Strauss, J.V., 2020, Calibrating the coevolution of Ediacaran life and environment: Proceeding of the National Academy of Science USA, v. 117, p. 16824-16830.

Rosenberg, M.J, Birgenheier, L.P., and Vanden Berg, M.D., 2015, Facies, stratigraphic architecture, and lake evolution of the oil shale bearing Green River Formation, eastern Uinta basin, Utah, *in* Smith, M.E., and Carroll A.R., eds., Stratigraphy and paleolimnology of the Green River Formation, Western USA: Syntheses in Limnogeology v. 1, Springer, Dordrect, p. 211-249.

Selby, D., and Creaser, R.A., 2003, Re-Os geochronology of organic rich sediments: an

811 evaluation of organic matter analysis methods: Chemical Geology, v. 200, p. 225-240.
812 Selby, D., and Creaser, R.A., 2005, Direct radiometric dating of hydrocarbon deposits using
813 rhenium-osmium isotopes: Science, v. 308, p. 1293-1295.
814 Selby, D., 2007, Direct rhenium-osmium age of the Oxfordian-Kimmeridgian boundary, Staffin
815 bay, Isle of Skye, UK, and the late Jurassic timescale: Norwegian Journal of Geology, v. 87,
816 p. 291-300.
817 Selby, D., Mutterlose, J., and Condon, D.J., 2009, U-Pb and Re-Os geochronology of the
818 Aptian/Albian and Cenomanian/Turonian stage boundaries: implications for timescale
819 calibration, osmium isotope seawater composition and Re-Os systematics in organic-rich
820 sediments: Chemical Geology, v. 265, p. 394-409.
821 Shirey, S.B., and Walker R.J., 1995, Carius tube digestion for low-blank Rhenium-Osmium
822 analysis: Analytical Chemistry, v. 67, p. 2136-2141.
823 Silliman, J.E., Meyers, P.A., and Bourbonniere, R.A., 1996, Record of postglacial organic matter
824 delivery and burial in sediments of Lake Ontario: Organic Geochemistry, v. 24, p. 463-472.
825 Smith, M.E., Carroll, A.R., and Singer, B.S., 2008, Synoptic reconstruction of a major ancient
826 lake system: Eocene Green River Formation, western United States: Geological Society of
827 America Bulletin, v. 120, p. 54-84.
828 Smith, M.E., and Carroll A.R., 2015, Introduction to the Green River Formation, *in* Smith,
829 M.E., and Carroll A.R., eds., Stratigraphy and paleolimnology of the Green River
830 Formation, Western USA: Syntheses in Limnogeology v. 1, Springer, Dordrect, p. 1-12.
831 Smoliar, M.I., Walker, R.J., and Morgan, J.W., 1996, Re-Os isotope constraints on the age of
832 Group IIA, IIIA, IVA, and IVB iron meteorites: Science, v. 271, p. 1099-1102.

833 Smoot, J.P., 1983, Depositional subenvironments in an arid closed basin: the Wilkins Peak
834 Member of the Green River Formation (Eocene), Wyoming, U.S.A: Sedimentology, v. 30, p.
835 801-827.
836 Stein, H., and Hannah, J., 2014, Rhenium-Osmium geochronology: sulfides, shales, oils, and
837 mantle, *in* Rink, W., and Thompson J., eds., Encyclopedia of Scientific Dating Methods,
838 Springer, Dordrecht, 25 p.
839 Stoeser, D.B., Green, G.N., Morath, L.C., Heran, D.W., Wilson, A.B., Moore, D.W., and Van
840 Gosen, B.S, 2005, Preliminary integrated geologic map databases for the United States -
841 Central states: Montana, Wyoming, Colorado, New Mexico, North Dakota, South Dakota,
842 Nebraska, Kansas, Oklahoma, Texas, Iowa, Missouri, Arkansas, and Louisiana: U.S.
843 Geological Survey Open-File Report 2005-1351.
844 Tissott, B.P, and Welte, D.H., 1984, Petroleum formation and occurrence 2nd Edition, Springer-
845 Verlag, Berlin, 699p.
846 Toma, J., Creaser, R.A., and Pană, D.I., 2020, High-precision Re-Os dating of Lower Juassic
847 shale packages from the Western Canadian Sedimentary Basin: Palaeogeography,
848 Palaeoclimatology, Palaeoecology, v. 560.
849 Vermeesch, P., 2018, IsoplotR: A free and open toolbox for geochronology: Geoscience
850 Frontiers, v. 9, p. 1479-1493.
851 Washburn, K.E., Birdwell, J.E., Foster, M., and Gutierrez, F., 2015, Detailed description of oil
852 shale organic and mineralogical heterogeneity via Fourier transform infrared microscopy:
853 Energy Fuels, v. 29, p. 4264-4271.
854 Xu, W., Ruhl, M., Jenkyns, H.C., Hesselbo, S.P., Riding, J.B., Selby, D., Naafs, B.D.A., Weijers,
855 J.W.H., Pancost, R.D., Tegelaar, E.W., and Idiz, E.F., 2017, Carbon sequestration in an

expanded lake system during the Toarcian oceanic anoxic event: Nature Geoscience, v. 10, p. 129-134.

Figure Captions

Fig. 1. A) Generalized stratigraphic column of the middle and upper Green River Formation (GRF) in the Coyote Wash #1 core highlighting the organic-rich (R) and organic-lean (L) zones in the lower Parachute Creek Member and positions of samples from the Douglas Creek Member (DC), R3, R4, R6, and Mahogany zone (MZ). Modified from Birgenheier and Vanden Berg (2011). Also shown are the positions of three volcanic ash layers dated by Smith and Carroll (2015). B) Plot of Os_i and isochron ages of samples from the Green River Formation plotted against position in the Coyote Wash #1 core. Age uncertainty and Os_i uncertainty bars are at the 2σ level. DC and MZ ages from Cumming et al. (2012). R4 age from Pietras et al. (2020). Two ages are shown for the R6 zone, one with all 20 samples, and one with four anomalous samples removed (see Figure 4). The Os_i value shown for the R6 zone was determined with the four anomalous samples removed. Also shown are the $^{40}Ar/^{39}Ar$ ages (italics) of three volcanic ash layers from Smith and Carroll (2015). B) Map showing the location of the Coyote Wash #1, Skyline 16, and PR15-7c cores in the eastern Uinta Basin, and the general bedrock lithology or age surrounding the basin. Sevier FTB - Sevier fold and thrust belt. Modified from Ludington et al. (2005) and Stoeser et al. (2005).

Fig. 2. A) Re-Os isochron plot of 10 samples from the R3 oil shale in the Skyline 16 core. B) Re-Os isochron plot of 10 samples from the R3 oil shale in the PR15-7c core. C) Re-Os isochron plot of all 20 samples from the R3 oil shale in both cores. D) Re-Os isochron plot of 10 samples

from the R6 oil shale in the Skyline 16 core. E) Re-Os isochron plot of 10 samples from the R6 oil shale in the PR15-7c core. F) Re-Os isochron plot of all 20 samples from the R6 oil shale in both cores (See also Fig. 5). Anomalous samples S6-7, S6-10, P6-3, and P6-7 are highlighted. See text for discussion.

Fig. 3. A) Pseudo-Van Krevelen diagram of all samples from the Green River Formation indicating the prevalence of Type I kerogen. B) Details of area in gray box of A. C) T_{max} versus HI cross-plot indicating that all samples of the Green River Formation are thermally immature. D) Details of area in gray box of C.

Fig. 4. Re-Os isochron plot of samples of the R6 zone from the Skyline 16 (black) and PR15-7c (gray). Anomalous samples S6-7, S6-10, P6-3, and P6-7 are highlighted (white), but were not used in creation of the isochron shown in the solid line. Dashed line is the isochron using all 20 samples.

Fig. 5. Isochron age versus stratigraphic position in the Coyote Wash #1 core of samples from the Green River Formation. Anomalous samples S6-7, S6-10, P6-3, and P6-7 were excluded for the R6 age (see Figure 4). The slope of the linear regression represents the average sedimentation rate.

Fig. 6. $^{187}Re/^{188}Os$ range versus age uncertainty cross-plot. The two curves correspond to modeled theoretical uncertainty using 10 (dashed) and 20 (solid) samples. Circles are the actual age uncertainty for each zone determined using *Isoplot v. 4.15*. Squares are the uncertainty for each zone using an initial $^{187}Os/^{188}Os$ value of 1.40, a depositional age of 49 Ma, local uncertainties, and a $^{187}Re/^{188}Os$ range determined by each sample set. See text for discussion.

Fig. 7. A) Carbon preference index (CPI) versus terrigenous-aquatic ratio (TAR) cross-plot of all EOM samples from the Green River Formation. B) Pristane/phytane versus β-carotane/n-C_{30} cross-plot of all EOM samples from the Green River Formation. Size of the symbol corresponds to the $^{187}Re/^{188}Os$ range in each set of samples.

Figure 1

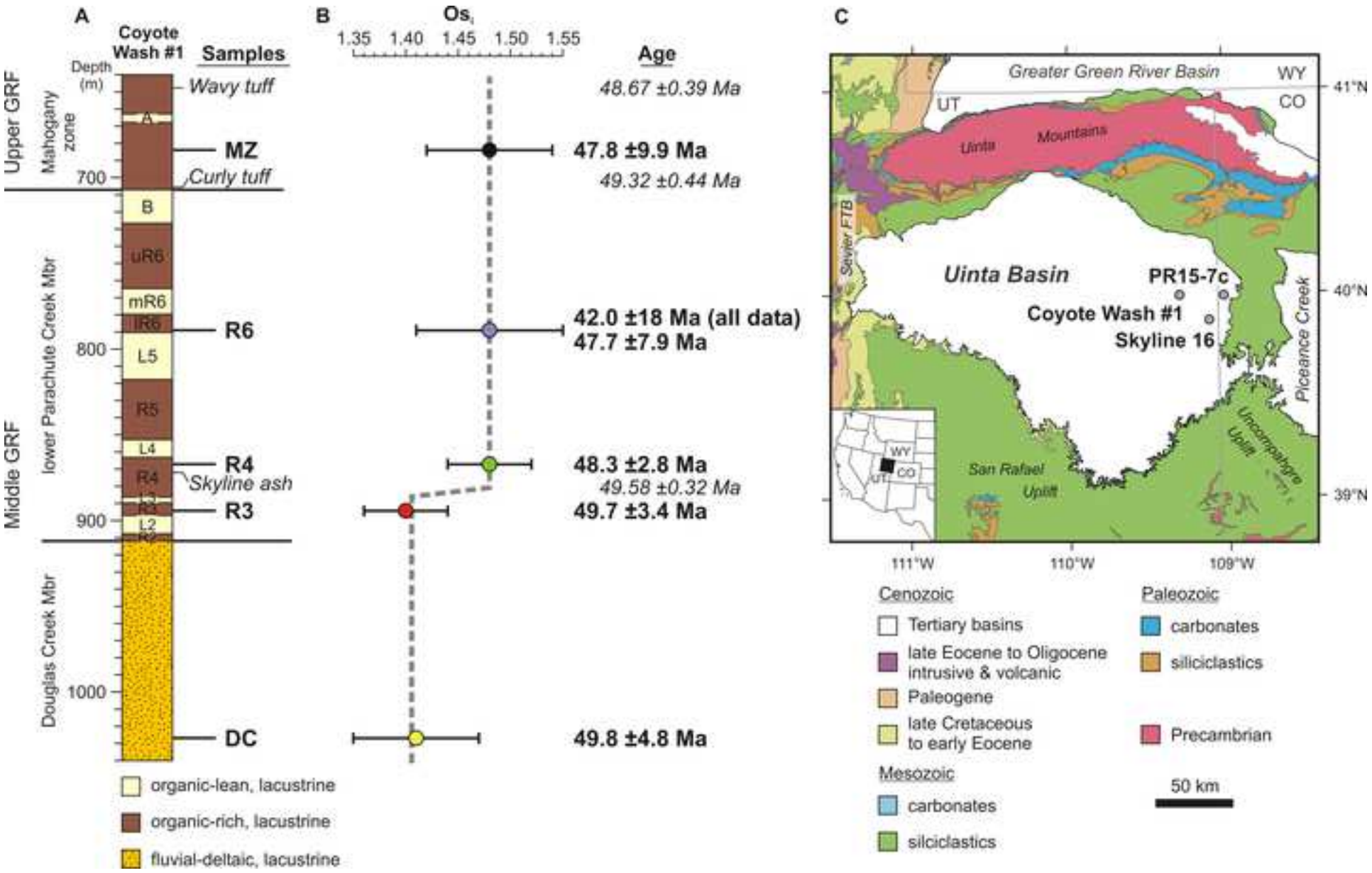

Figure 2

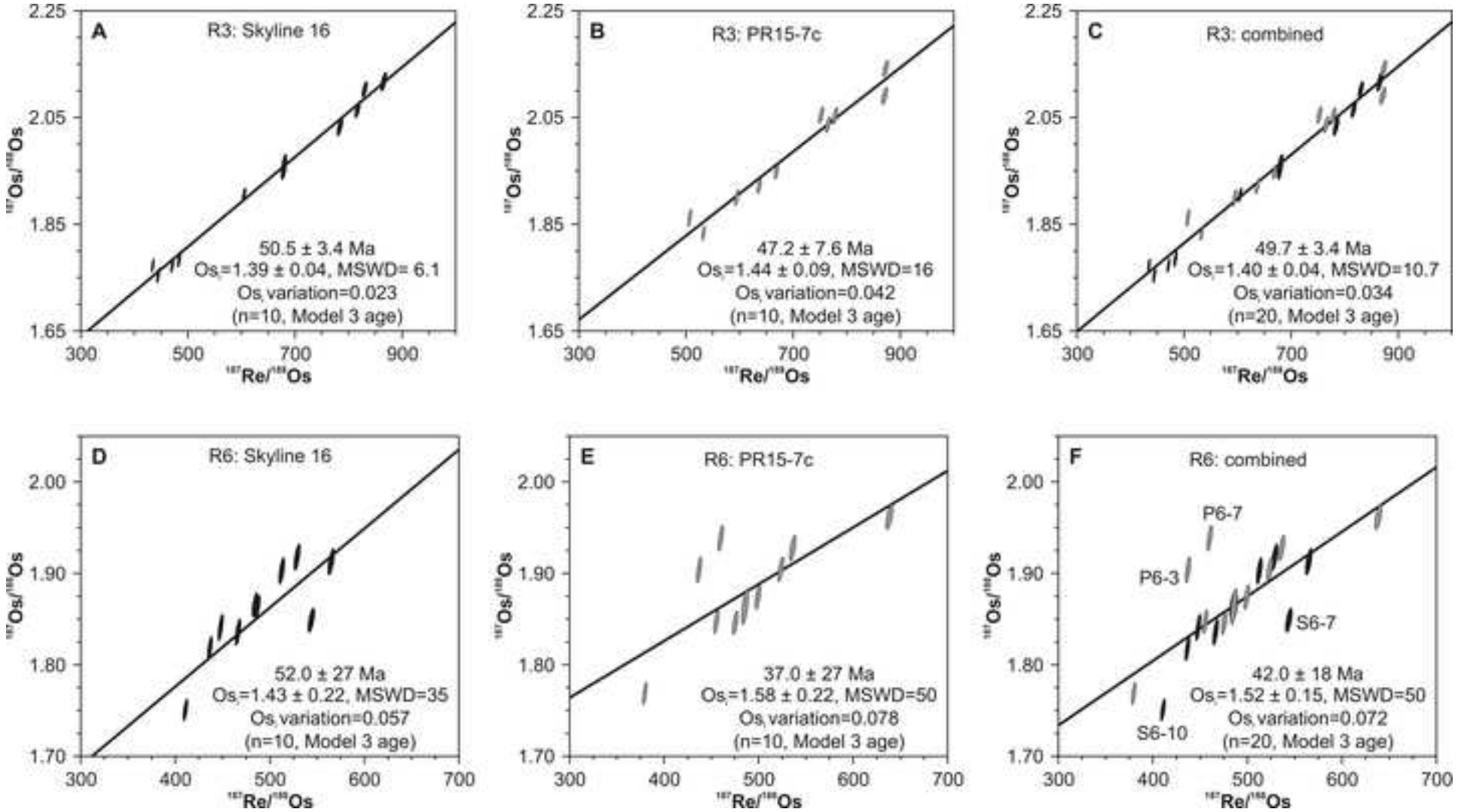

Figure 3

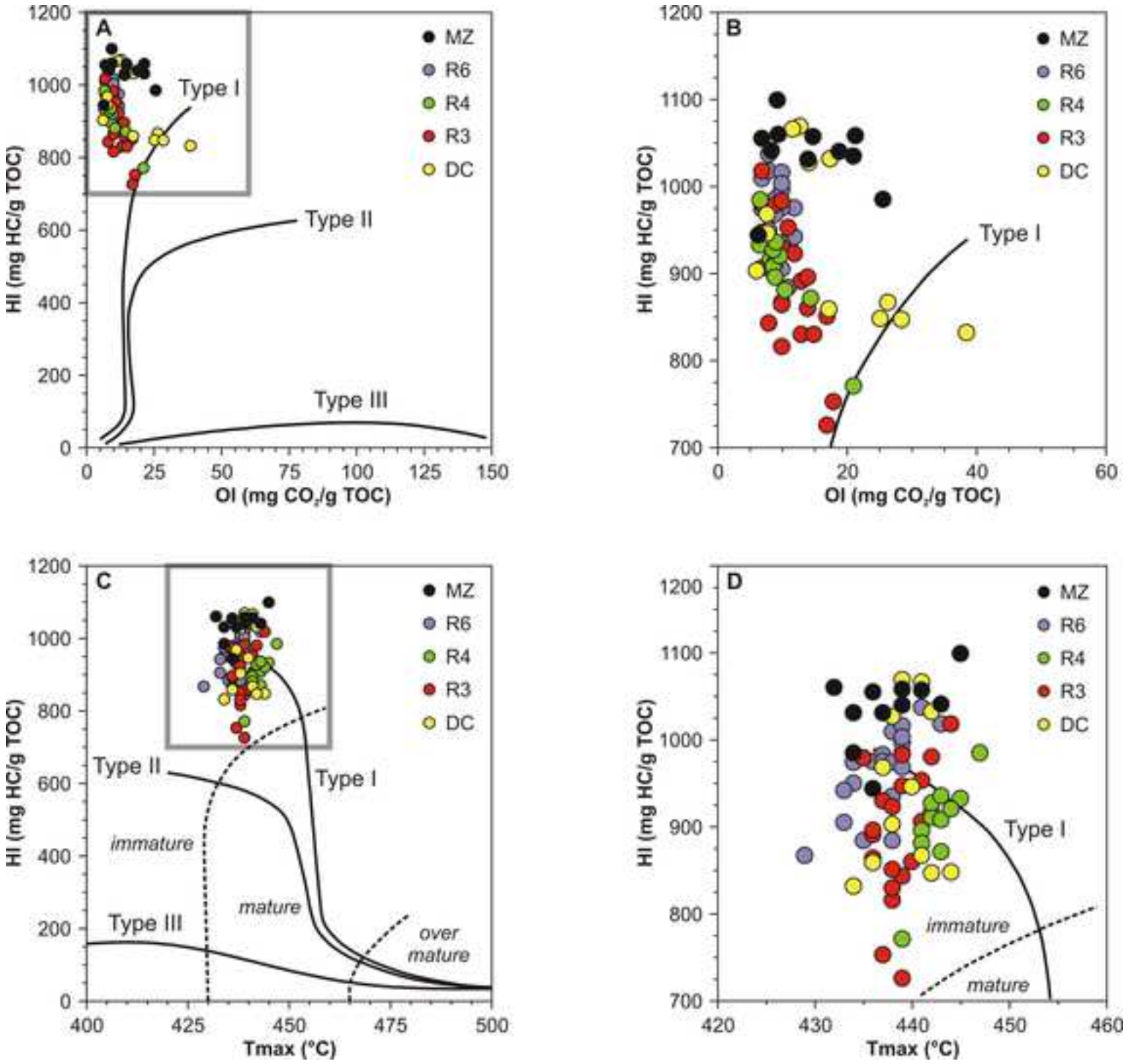

Figure 4

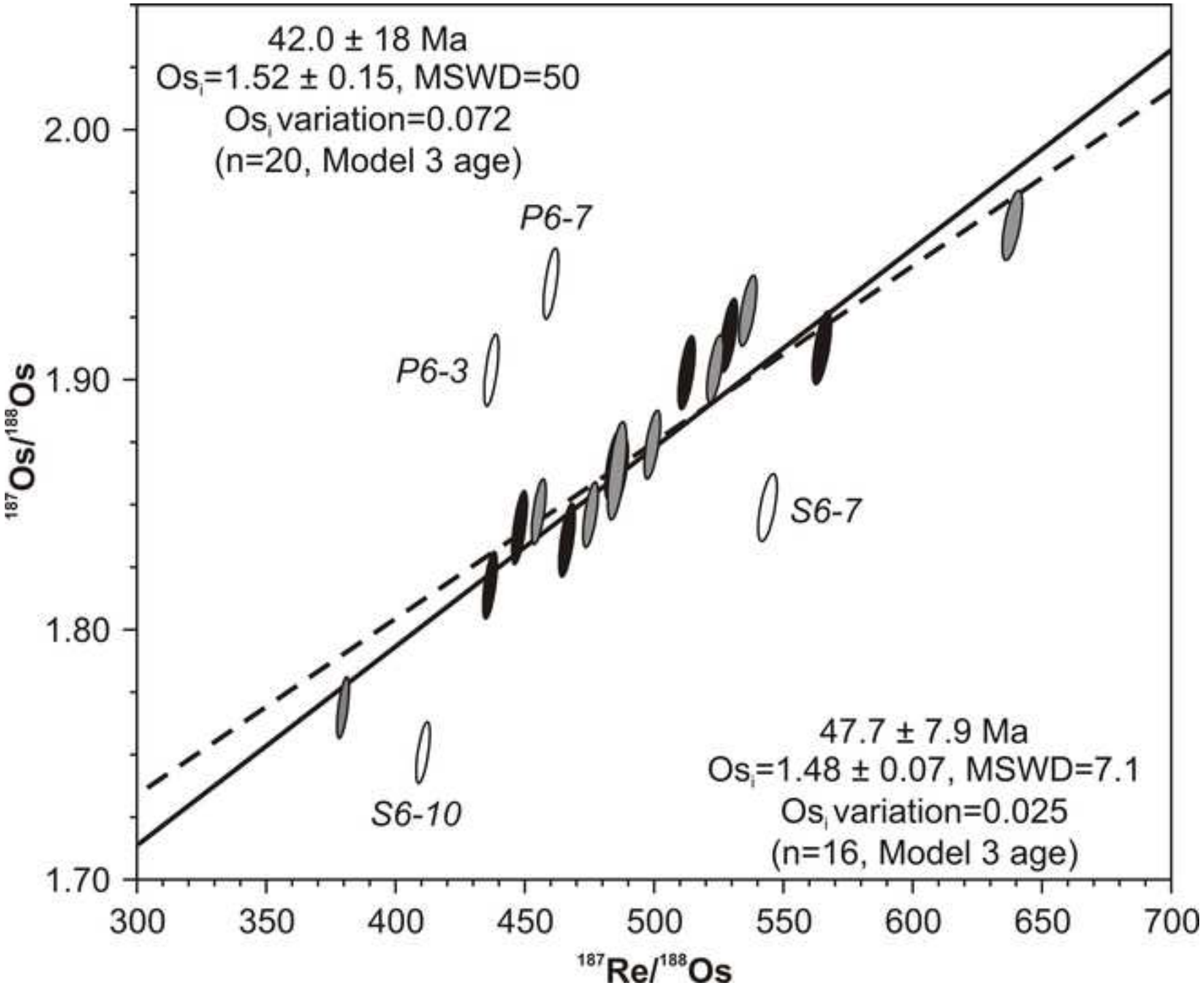

Figure 5

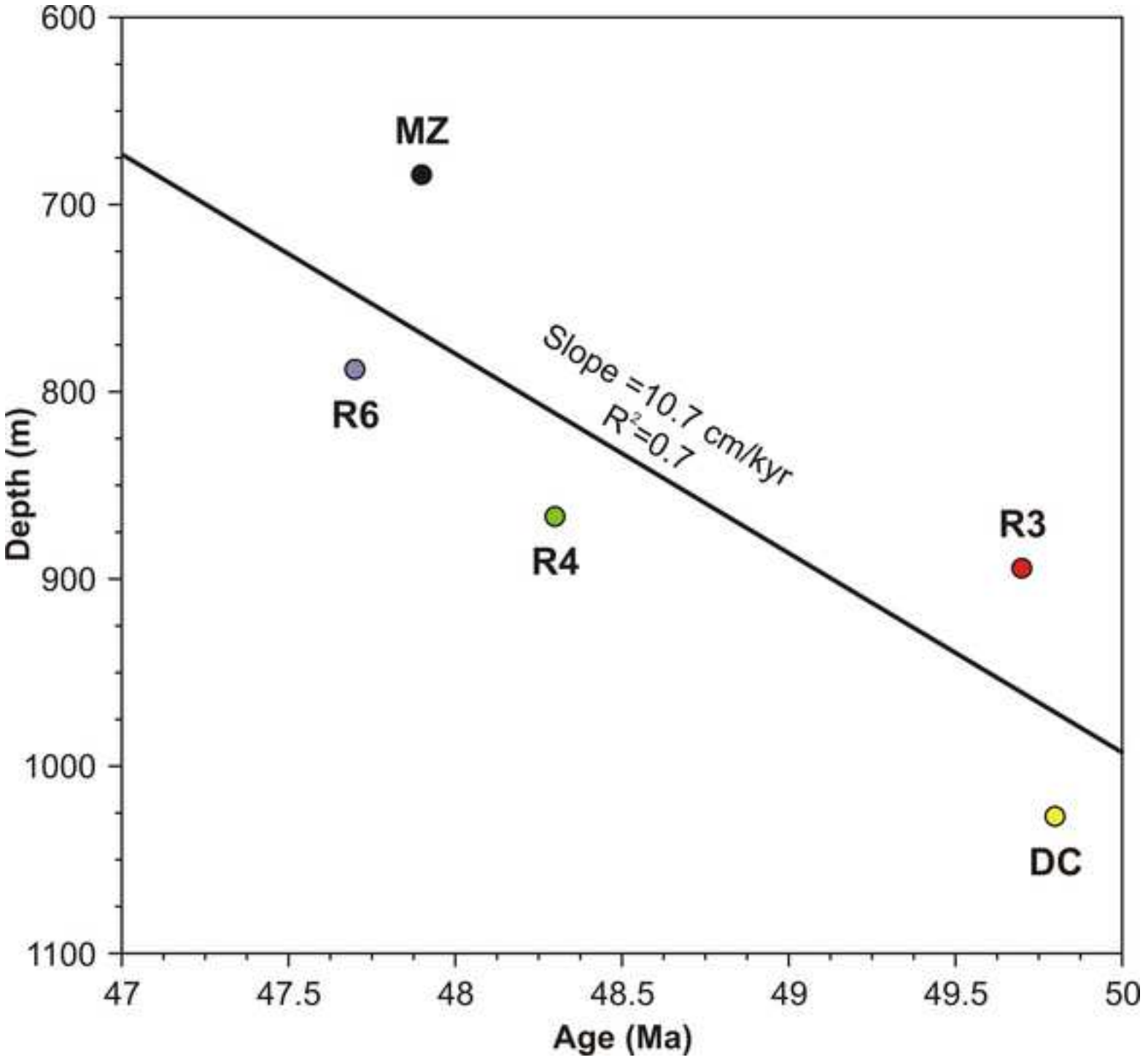

Figure 6

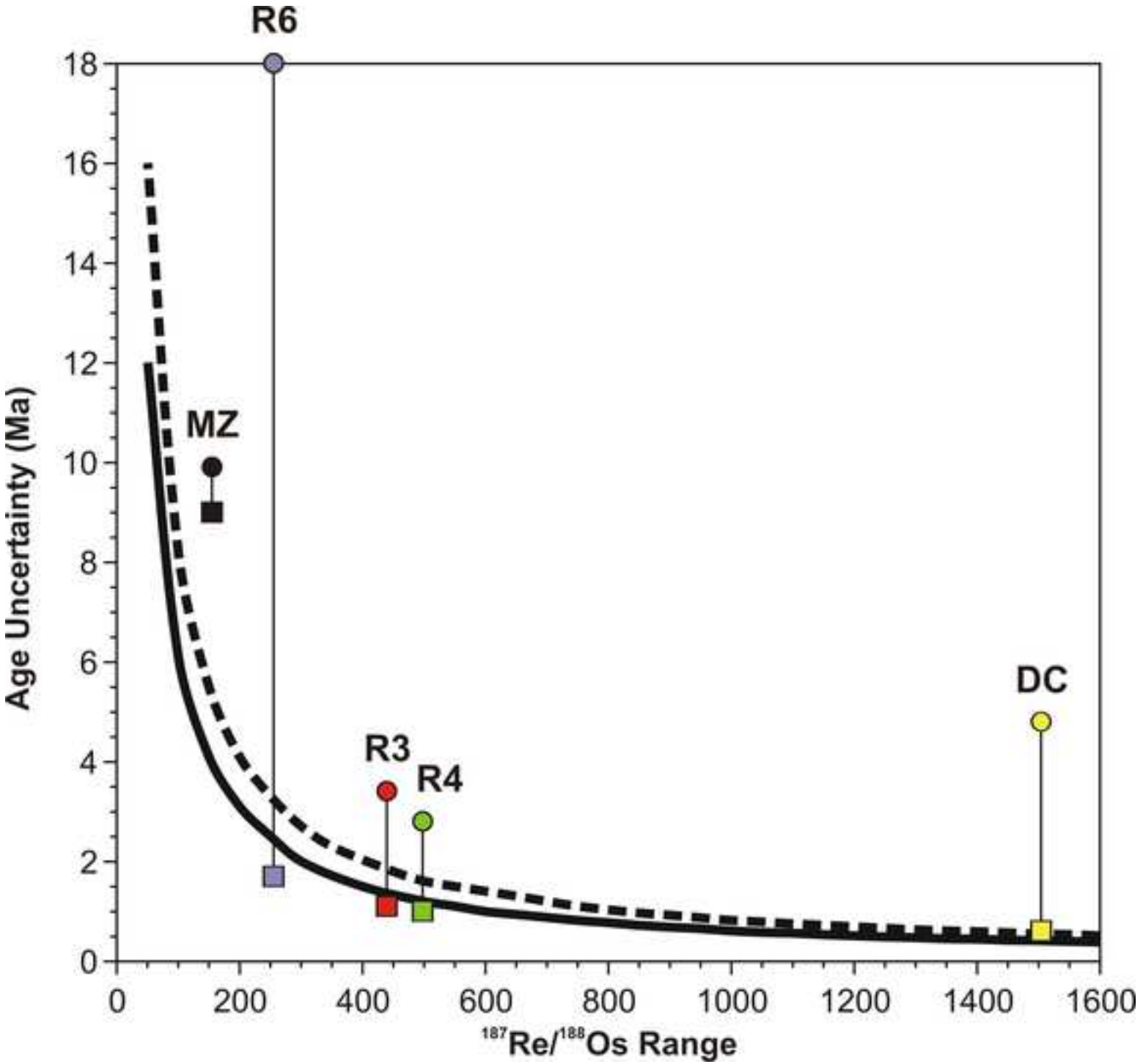

Figure 7

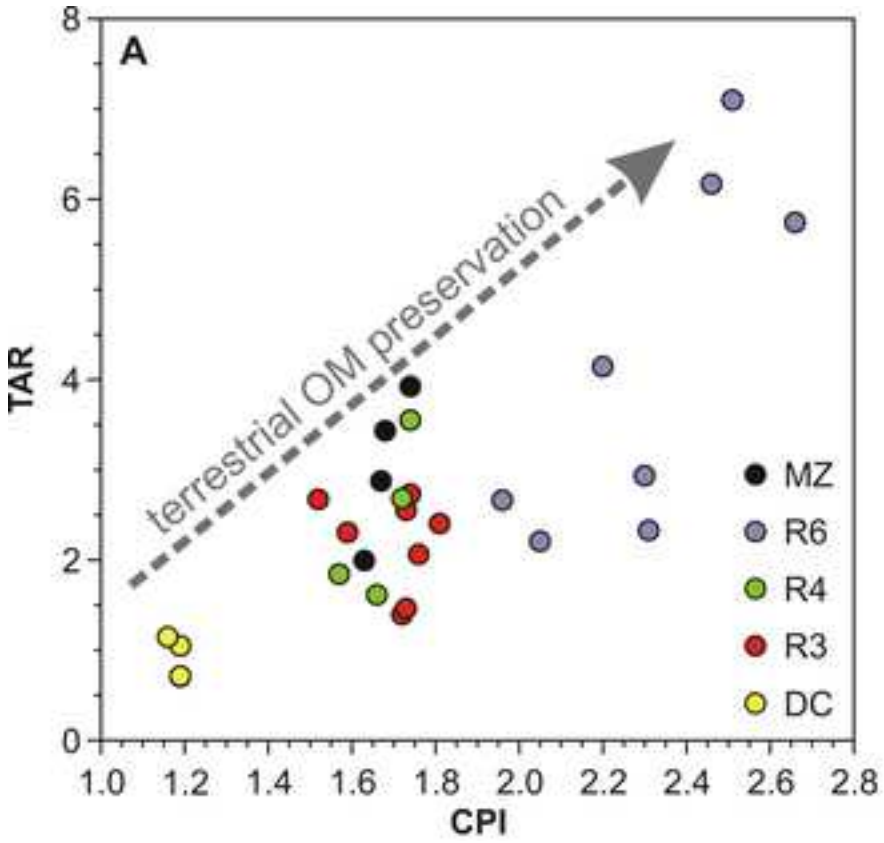

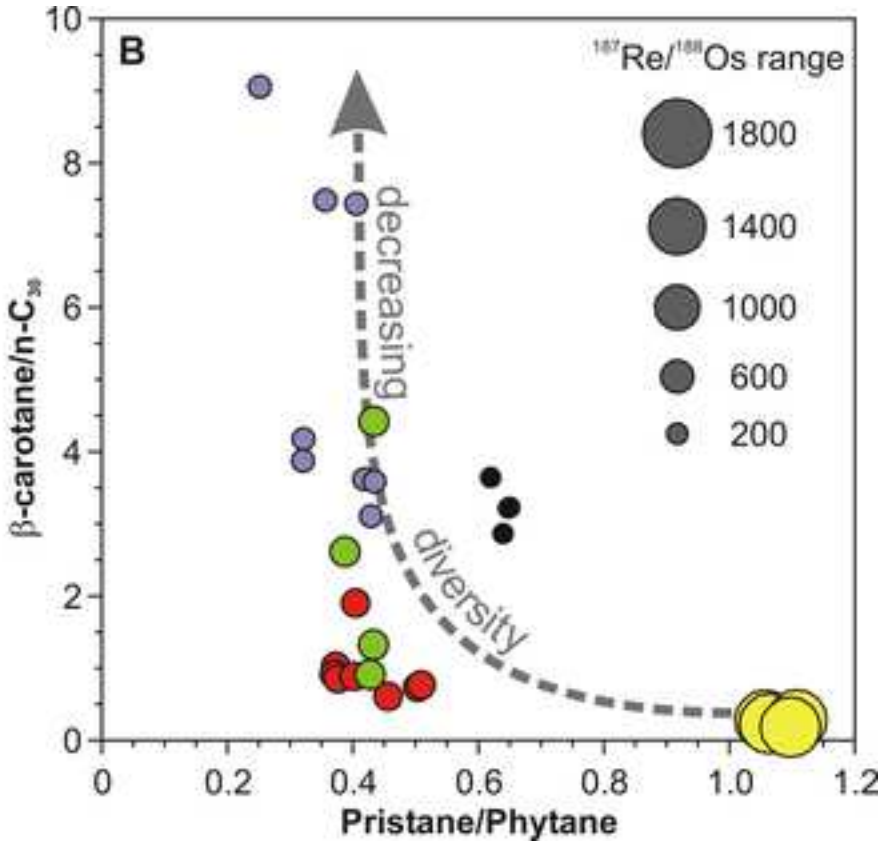

Table 1 Click here to access/download;Table;Pietras_et_al_Table_1.xlsx

Table 1 Re-Os isotope data

Sample name	Depth (m)	Re (ppb)	±	Os (ppt)	±	^{192}Os (ppt)	±	^{187}Re/^{188}Os	±	^{187}Os/^{188}Os	±	rho[a]	% Re blank	% ^{187}Os blank	% ^{188}Os blank	Os_i[b]	±
PR15-7c																	
R6 zone																	
P6-1	117.33	20.57	0.05	264.0	1.3	89.0	0.4	459.7	2.2	1.847	0.011	0.624	0.31	0.02	0.15	1.47	0.01
P6-2	117.28	20.54	0.05	231.4	1.2	77.6	0.3	527.0	2.6	1.905	0.011	0.635	0.31	0.02	0.17	1.47	0.01
P6-3	117.22	20.61	0.05	277.0	1.4	92.8	0.4	441.7	2.2	1.904	0.012	0.623	0.31	0.02	0.15	1.54	0.01
P6-4	117.14	17.27	0.04	208.5	1.3	70.2	0.4	489.6	3.0	1.864	0.016	0.599	0.37	0.02	0.19	1.46	0.02
P6-5	117.06	19.36	0.05	227.7	1.2	76.6	0.3	503.0	2.5	1.874	0.011	0.634	0.33	0.02	0.18	1.46	0.01
P6-6	117.00	18.56	0.05	204.7	1.1	68.4	0.3	539.4	2.7	1.928	0.012	0.645	0.34	0.02	0.20	1.49	0.01
P6-7	116.94	16.96	0.04	217.6	1.1	72.7	0.3	464.4	2.3	1.939	0.012	0.632	0.37	0.02	0.19	1.56	0.01
P6-8	116.88	25.86	0.06	241.3	1.2	80.4	0.3	640.1	3.1	1.962	0.011	0.634	0.24	0.02	0.17	1.44	0.01
P6-9	116.76	23.65	0.06	291.0	1.4	98.1	0.4	479.5	2.3	1.846	0.011	0.621	0.27	0.01	0.14	1.45	0.01
P6-10	116.58	16.69	0.04	253.5	1.2	86.2	0.4	385.2	1.9	1.769	0.010	0.628	0.38	0.02	0.16	1.45	0.01
R3 zone																	
P3-1	185.77	25.78	0.06	199.5	1.1	65.8	0.3	779.1	4.0	2.053	0.013	0.644	0.23	0.02	0.20	1.42	0.01
P3-2	185.68	13.48	0.04	157.1	0.9	52.9	0.3	507.3	2.9	1.862	0.013	0.640	0.44	0.03	0.25	1.45	0.01
P3-3	185.61	21.63	0.05	173.3	0.9	57.2	0.3	753.0	4.0	2.055	0.013	0.659	0.28	0.02	0.24	1.44	0.01
P3-4	185.54	25.26	0.06	175.4	1.0	57.7	0.3	871.5	4.7	2.091	0.013	0.652	0.24	0.02	0.23	1.38	0.01
P3-5	185.49	20.57	0.05	161.7	0.9	53.4	0.2	765.7	4.0	2.037	0.012	0.674	0.29	0.02	0.25	1.41	0.01
P3-6	185.40	26.91	0.07	187.5	1.0	61.3	0.3	873.6	4.4	2.142	0.013	0.658	0.22	0.02	0.22	1.43	0.01
P3-7	185.30	21.77	0.05	217.1	1.2	72.8	0.3	595.0	3.1	1.900	0.012	0.631	0.28	0.02	0.18	1.41	0.01
P3-8	185.22	16.82	0.04	185.9	0.9	62.8	0.3	533.0	2.7	1.833	0.011	0.651	0.36	0.02	0.21	1.40	0.01
P3-9	185.16	22.13	0.05	206.5	1.1	69.1	0.3	637.2	3.2	1.922	0.011	0.643	0.27	0.02	0.19	1.40	0.01
P3-10	185.10	29.46	0.07	262.5	1.3	87.6	0.4	669.4	3.3	1.949	0.011	0.626	0.20	0.02	0.15	1.40	0.01
Skyline 16																	
R6 zone																	
S6-1	217.68	20.07	0.05	224.2	1.2	75.0	0.3	532.1	2.7	1.918	0.012	0.631	0.32	0.02	0.18	1.48	0.01
S6-2	217.56	15.37	0.04	200.3	1.1	67.6	0.3	452.4	2.4	1.841	0.012	0.639	0.41	0.02	0.2	1.47	0.01
S6-3	217.47	22.01	0.05	253.2	1.3	84.9	0.4	516.1	2.6	1.903	0.012	0.614	0.29	0.02	0.16	1.48	0.01
S6-4	217.34	14.72	0.04	178.3	0.9	60.0	0.3	488.1	2.5	1.866	0.011	0.654	0.43	0.02	0.22	1.47	0.01
S6-5	217.25	15.62	0.04	188.1	1.0	63.3	0.3	490.8	2.5	1.863	0.011	0.644	0.4	0.02	0.21	1.46	0.01
S6-6	217.19	15.04	0.04	188.3	1.0	63.6	0.3	470.5	2.5	1.836	0.012	0.632	0.42	0.02	0.21	1.45	0.01
S6-7	217.13	18.61	0.05	200.8	1.0	67.7	0.3	546.9	2.9	1.849	0.011	0.614	0.34	0.02	0.2	1.40	0.01
S6-8	217.07	21.64	0.05	226.5	1.2	75.8	0.3	567.6	2.9	1.913	0.012	0.636	0.29	0.02	0.18	1.45	0.01
S6-9	216.95	22.37	0.06	298.2	1.5	100.9	0.4	441.2	2.2	1.818	0.011	0.612	0.28	0.01	0.13	1.46	0.01
S6-10	216.73	15.75	0.04	221.2	1.1	75.4	0.3	415.7	2.1	1.751	0.010	0.637	0.25	0.02	0.14	1.41	0.01
R3 zone																	
S3-1	285.48	23.91	0.06	176.6	0.9	58.2	0.3	817.2	4.2	2.065	0.013	0.654	0.25	0.02	0.23	1.40	0.01
S3-2	285.44	16.66	0.04	127.8	0.7	42.3	0.2	784.3	4.6	2.033	0.014	0.680	0.36	0.03	0.32	1.39	0.01
S3-3	285.38	13.00	0.03	161.5	0.8	54.9	0.3	471.0	2.5	1.773	0.011	0.662	0.46	0.03	0.25	1.39	0.01
S3-4	285.31	11.59	0.03	140.3	0.8	47.6	0.2	484.0	2.8	1.785	0.013	0.649	0.52	0.03	0.28	1.39	0.01
S3-5	285.25	11.28	0.03	148.2	0.8	50.5	0.3	444.4	2.5	1.755	0.012	0.651	0.53	0.03	0.27	1.39	0.01
S3-6	285.19	24.05	0.06	168.6	1.0	55.3	0.3	865.9	4.8	2.118	0.015	0.636	0.25	0.02	0.24	1.41	0.02
S3-7	285.13	32.65	0.08	238.2	1.2	78.2	0.3	830.5	4.1	2.103	0.012	0.637	0.18	0.02	0.17	1.42	0.01
S3-8	285.07	19.48	0.05	262.4	1.3	89.2	0.4	434.5	2.2	1.773	0.011	0.624	0.31	0.02	0.15	1.42	0.01
S3-9	285.01	30.59	0.08	300.1	1.5	100.6	0.4	605.0	2.9	1.905	0.011	0.614	0.20	0.01	0.13	1.41	0.01
S3-10	284.95	29.08	0.07	255.4	1.7	85.1	0.5	679.7	4.5	1.958	0.019	0.579	0.21	0.02	0.16	1.40	0.02

All uncertainties are reported at 2σ

[a] rho is the associated error correlation at 2σ (Ludwig, 1980)

[b] Os_i is the initial $^{187}Os/^{188}Os$ isotopic ratio calculated at 49 Ma

Table 2 Initial $^{187}Os/^{188}Os$ values

Sample name	Depth (m)	Os_i [c]	±
PR15-7c[a]			
R4 zone			
PR1	166.50	1.46	0.01
PR2	166.55	1.48	0.01
PR3	166.60	1.48	0.01
PR4	166.65	1.47	0.01
PR5	166.68	1.48	0.02
PR6	166.75	1.46	0.02
PR7	166.80	1.46	0.01
Skyline 16[a]			
R4 zone			
SL1	269.77	1.44	0.01
SL2	269.82	1.46	0.01
SL3	269.88	1.50	0.01
SL4	269.92	1.50	0.01
SL5	269.98	1.48	0.01
SL6	270.03	1.47	0.01
SL7	270.08	1.48	0.01
SL8	270.13	1.49	0.01
SL9	270.18	1.44	0.01
SL10	270.23	1.46	0.01
SL11	270.28	1.47	0.01
SL12	270.33	1.48	0.01
Coyote Wash 1[b]			
Mahogany zone			
CW1-05	682.50	1.47	0.02
CW1-06	682.70	1.47	0.01
CW1–07	682.80	1.47	0.01
CW1–09	683.20	1.47	0.05
CW1–10	683.40	1.48	0.02
CW1–12	683.60	1.48	0.04
CW1–13	683.70	1.49	0.02
CW1–14	683.90	1.47	0.03
CW1–15	684.30	1.48	0.04
CW1–16	684.50	1.49	0.02
CW1–20	684.90	1.47	0.05
CW1–22	685.20	1.48	0.02
CW1–23	685.40	1.48	0.03
Douglas Creek Mbr.			
CW1-40	1026.00	1.41	0.01
CW1-41	1026.10	1.39	0.02
CW1-42	1026.20	1.39	0.02
CW1-44	1026.50	1.30	0.02
CW1-45	1026.60	1.45	0.01
CW1-46	1026.80	1.47	0.01
CW1-48	1027.00	1.41	0.03
CW1-49	1027.20	1.39	0.02
CW1-50	1027.40	1.41	0.03
CW1-51	1027.50	1.45	0.03
CW1-53	1027.70	1.48	0.02
CW1-54	1027.80	1.40	0.01
CW1-55	1028.00	1.45	0.01

All uncertainties are reported at 2σ

[a] R4 zone sample names from Pietras et al. (2020)

[b] Coyote Wash #1 sample names from Cumming et al. (2012)

[c] Os_i is the initial $^{187}Os/^{188}Os$ isotopic ratio calculated at 49 Ma

Table 3 Programmed pyrolysis and total organic carbon (TOC) data

Sample name	Depth (m)	TOC (wt%)	S1 (mg hydrocarbons/g of rock)	S2 (mg hydrocarbons/g of rock)	S3 (mg CO_2/g of rock)	Tmax (°C)	HI (mg-HC/g-TOC)	OI (mg-CO_2/g-TOC)	PI[b]
PR15-7c									
R6 zone									
P6-1	117.33	7.62	2.52	74.27	0.92	436	975	12	0.03
P6-2	117.28	7.82	2.22	78.88	0.57	438	1009	7	0.03
P6-3	117.22	7.58	2.43	74.52	0.54	437	983	7	0.03
P6-4	117.14	3.93	2.05	35.58	0.39	433	905	10	0.05
P6-5	117.06	4.33	2.66	37.58	0.43	429	867	10	0.07
P6-6	117.00	4.59	2.41	40.54	0.5	438	884	11	0.06
P6-7	116.94	6.66	2.61	69.07	0.51	441	1037	8	0.04
P6-8	116.88	7.97	1.81	81.15	0.65	443	1018	8	0.02
P6-9	116.76	8.56	2.45	84.34	0.8	439	985	9	0.03
P6-10	116.58	9.97	2.22	99.25	0.99	439	996	10	0.02
R4 zone[a]									
PR3	166.60	6.17	0.63	56.56	0.51	442	917	8	0.01
PR6	166.75	4.97	0.51	45.26	0.44	442	911	9	0.01
R3 zone									
P3-1	185.77	4.62	0.84	38.94	0.38	439	843	8	0.02
P3-2	185.68	2.44	0.53	17.71	0.41	439	726	17	0.03
P3-3	185.61	3.13	0.76	26.02	0.41	438	830	13	0.03
P3-4	185.54	3.31	0.96	28.55	0.33	436	864	10	0.03
P3-5	185.49	3.66	0.87	29.85	0.35	438	816	10	0.03
P3-6	185.40	4.31	1.02	40.08	0.41	437	930	10	0.02
P3-7	185.30	7.99	1.99	75.65	0.55	439	947	7	0.03
P3-8	185.22	6.25	1.36	56.61	0.41	441	906	7	0.02
P3-9	185.16	7.34	1.44	71.93	0.51	442	980	7	0.02
P3-10	185.10	9.4	1.71	95.69	0.69	444	1018	7	0.02
Skyline 16									
R6 zone									
S6-1	217.68	8.42	1.81	85.52	0.83	439	1016	10	0.02
S6-2	217.56	6.21	2.01	58.99	0.51	434	950	8	0.03
S6-3	217.47	7.73	2.23	75.37	0.67	434	974	9	0.03
S6-4	217.34	3.62	2.22	34.13	0.43	433	942	12	0.06
S6-5	217.25	3.8	2.2	33.6	0.41	435	884	11	0.06
S6-6	217.19	5.55	2	51.96	0.53	438	935	10	0.04
S6-7	217.13	5.19	1.74	50.61	0.51	437	975	10	0.03
S6-8	217.07	8.02	1.72	78.06	0.57	438	974	7	0.02
S6-9	216.95	10.03	2.61	97.14	0.95	439	968	9	0.03
S6-10	216.73	6.98	1.31	69.96	0.71	439	1003	10	0.02
R4 zone[a]									
SL1	269.77	6.45	0.89	58.56	0.56	443	908	9	0.01
SL2	269.82	5.63	0.67	52.5	0.37	445	933	7	0.01
SL3	269.88	5.01	0.6	44.88	0.45	441	896	9	0.01
SL4	269.93	5.26	0.62	48.42	0.51	444	921	10	0.01
SL6	270.03	8.65	0.99	85.18	0.58	447	985	7	0.01
SL7	270.08	3.65	0.34	31.81	0.53	443	872	15	0.01
SL8	270.13	2.8	0.26	21.59	0.59	439	771	21	0.01
SL10	270.23	4.18	0.33	36.82	0.44	441	881	11	0.01
SL11	270.28	5.98	0.72	55.44	0.52	442	927	9	0.01
SL12	270.33	6.05	0.55	56.61	0.55	443	936	9	0.01
R3 zone									
S3-1	285.48	2.87	0.49	25.58	0.37	436	891	13	0.02
S3-2	285.44	2.05	0.34	15.44	0.36	437	753	18	0.02
S3-3	285.38	2.77	0.36	23.83	0.38	440	860	14	0.01
S3-4	285.31	2.78	0.39	23.64	0.46	438	851	17	0.02
S3-5	285.25	2.62	0.44	21.76	0.4	438	830	15	0.02
S3-6	285.19	2.68	0.79	24.03	0.37	436	896	14	0.03
S3-7	285.13	7.47	2.59	73.15	0.64	435	979	9	0.03
S3-8	285.07	3.83	0.9	35.4	0.45	438	923	12	0.02
S3-9	285.01	8.82	2.31	86.64	0.86	439	983	10	0.03
S3-10	284.95	5.09	0.9	48.52	0.54	441	953	11	0.02

[a] R4 zone sample names from Pietras et al. (2020)

[b] Production index (PI) = S1/(S1 + S2)

Table 4 Extractable organic matter (EOM) biomarker data

Sample name	Depth (m)	EOM (wt.%)	CPI[c]	TAR[d]	Pr/Ph[e]	βC[f]/n-C30
PR15-7c						
R6 zone						
P6-1	117.33	0.649	1.96	2.66	0.41	7.44
P6-4	117.14	0.734	2.66	5.74	0.32	3.87
P6-7	116.94	1.317	2.46	6.17	0.32	4.18
P6-10	116.58	0.600	2.31	2.33	0.25	9.06
R3 zone						
P3-1	185.77	0.308	1.76	2.06	0.38	0.86
P3-4	185.54	0.590	1.73	2.55	0.40	0.89
P3-7	185.30	0.775	1.81	2.40	0.37	0.92
P3-10	185.10	0.646	1.74	2.73	0.37	1.03
Skyline 16						
R6 zone						
S6-1	217.68	0.648	2.30	2.94	0.43	3.59
S6-4	217.34	0.759	2.51	7.10	0.43	3.11
S6-7	217.13	0.797	2.20	4.14	0.42	3.62
S6-10	216.73	0.559	2.05	2.21	0.36	7.49
R4 zone[a]						
SL1	269.77	0.322	1.74	3.55	0.43	0.91
SL4	269.93	0.252	1.57	1.84	0.43	1.33
SL8	270.13	0.219	1.72	2.68	0.39	2.61
SL12	270.33	0.309	1.66	1.61	0.43	4.43
R3 zone						
S3-1	285.48	0.230	1.73	1.46	0.51	0.77
S3-4	285.31	0.377	1.72	1.39	0.50	0.73
S3-7	285.13	1.180	1.59	2.31	0.40	1.90
S3-10	284.95	0.377	1.52	2.67	0.46	0.61
Coyote Wash 1[b]						
Mahogany Zone						
CW1-05	682.5	2.636	1.63	1.99	0.62	3.65
CW1–10	683.4	2.320	1.67	2.87	0.65	3.22
CW1–15	684.3	1.805	1.74	3.92	0.65	3.23
CW1–22	685.2	2.842	1.68	3.43	0.64	2.87
Douglas Creek Mbr.						
CW1-40	1026.0	0.472	1.19	0.71	1.06	0.23
CW1-45	1026.6	0.871	1.19	1.05	1.06	0.28
CW1-50	1027.4	1.119	1.19	0.71	1.10	0.18
CW1-55	1028.0	1.417	1.16	1.14	1.11	0.29

[a] R4 zone sample names from Pietras et al. (2020)

[b] Coyote Wash #1 sample names from Cumming et al. (2012)

[c] Carbon Preference Index using Marzi et al., 1993

[d] Terrigenous-Aquatic Ratio using Bourbonniere and Meyers, 1996

[e] pristane/phytane ratio

[f] β-carotane

Table 5 Average analytical uncertainty modeling parameters

Zone	Uncertainty[a]			Number of
	$^{187}Re/^{188}Os$	$^{187}Os/^{188}Os$	rho	samples
Mahogany Zone	4.4	0.029	0.695	13
R6 Zone	2.5	0.011	0.629	20
R4 Zone	4.1	0.013	0.634	19
R3 Zone	3.6	0.013	0.640	20
Douglas Creek	5.3	0.020	0.706	13
All data	3.9	0.016	0.657	20/10

[a]2σ average for each zone

Table 6 Os_i variance

Zone	49Ma[a]	Isoplot v. 4.15[b]	IsoplotR[b]
Mahogany Zone	0.02	na[c]	0.002
R6 Zone	0.16	0.072	0.068
R4 Zone	0.06	0.030	0.028
R3 Zone	0.07	0.034	0.032
Douglas Creek	0.18	0.095	0.086

[a]total Os_i variance calculated at 49 Ma for all samples

[b]2σ

[c]variance not calculated for Model 1 age